SUPPLEMENTARY INFORMATION

The response of vegetation to drought time-scales across global land biomes

Sergio M. Vicente-Serrano[a], Célia Gouveia[b,c], Jesús Julio Camarero[d], Santiago Beguería[e], Ricardo Trigo[b,f], Juan I. López-Moreno[a], César Azorín-Molina[a], Edmond Pasho[a], Jorge Lorenzo-Lacruz[a], Jesús Revuelto[a], Enrique Morán-Tejeda[a] and Arturo Sanchez-Lorenzo[g]

[a]Instituto Pirenaico de Ecología, Consejo Superior de Investigaciones Científicas, Zaragoza, Spain 50059; [b]CGUL, IDL, Faculdade de Ciências, Universidade de Lisboa, Portugal; [c]Escola Superior de Tecnologia, Instituto Politécnico de Setúbal, Setúbal, Portugal; [d]ARAID-Instituto Pirenaico de Ecología; [e]Estación Experimental de Aula Dei, Consejo Superior de Investigaciones Científicas, Zaragoza, Spain; [f]Departamento de Engenharias, Universidade Lusófona, Lisboa, Portugal; [g]Institute for Atmospheric and Climate Science, ETH Zurich, Zurich, Switzerland

This document contains:

1. Supplemental material and methods

1.1. Drought index and dataset

Substantial efforts have been devoted for developing methods to quantify drought severity. The main efforts have been directed at developing drought indices that enable earlier identification of droughts, and quantification of their severity and spatial extent. Several drought indices were developed during the 20th century, based on a range of variables and parameters (S1-S4).

Most studies related to drought analysis have been conducted using either (i) the Palmer Drought Severity Index (PDSI) (S5), based on a soil water balance equation, or (ii) the Standardized Precipitation Index (SPI) (S6), based on a precipitation probabilistic approach. The PDSI has numerous deficiencies (6) but the main problem for the identification of drought impacts is that the PDSI has a fixed temporal scale (S7) whereas it is commonly accepted that drought is a multi-scalar phenomenon since the period from the water shortages to impacts in a given system differs noticeably. Drought is a phenomenon that may occur simultaneously across multiple temporal scales (e.g., a short period of particular dryness embedded within a long-term drought). Therefore, "multiple" refers to numerous, temporal periods that may or may not overlap. Thus, drought indices must be associated with a specific time scale to be useful for monitoring drought impacts of different nature. This explains the wide acceptance of the SPI, which is comparable in time and space (S7,S8), and can be calculated at different time scales. The SPI has been accepted by the World Meteorological Organization as the reference drought index (S9). Thus, a number of studies have demonstrated variation in the response at different time scales of the SPI to different hydrological (S10-S13); agricultural (S14,S15) and ecological variables (11,12,15).

The main criticism for the SPI is that its calculation is based only on precipitation data. The index does not consider other variables that can influence droughts, mainly the evapotranspirative demand by the atmosphere. Abramopoulos et al. (S16) used a general circulation model experiment to show that evaporation and transpiration can consume up to 80% of rainfall. The role of warming-induced drought stress is evident in recent studies that have analysed drought impacts on net primary production and tree mortality (S17-S21). The strong role of temperatures on the drought severity was evident in the devasting 2003 central European heat wave, in which extreme high temperatures dramatically increased evapotranspiration and exacerbated summer drought stress (S22), drastically reducing Aboveground Net Primary Production (ANPP) (5). Similar patterns were observed in the summer 2010 with a strong heat wave that increased drought stress in forests and produced large forest fires in eastern Europe and Russia (S23). Thus, empirical studies have demonstrated that higher temperatures increase drought stress and enhance forest mortality under precipitation shortages (13). Warming processes are also probably the triggering factor of the decline in world agricultural productions observed in the last years (S24). Thus, to illustrate how warming processes are reinforcing drought stress and related ecological impacts worldwide, Breshears et al. (7) enunciated the term global-change-type drought to refer to drought under global warming conditions.

Therefore, the use of drought indices which include temperature data in their formulation (such as the PDSI) is preferable to identify drought impacts on vegetation activity and growth. However, the PDSI lacks the multi-scalar character, essential to assess the different times of response of global vegetation communities to drought. For this reason, in this study we used a recently formulated drought index: the Standardized Precipitation Evapotranspiration Index (SPEI) based on precipitation (P) and Potential Evapotranspiration (PET) (17). The SPEI combines the sensitivity of PDSI to changes in evaporation demand (caused by temperature fluctuations and trends) with the multi-temporal nature of the SPI.

The SPEI is calculated by means of a climatic water balance i.e. the difference between precipitation and PET:

$$D = P - PET,$$

The calculated D values are aggregated at various time scales:

$$D_n^k = \sum_{i=0}^{k-1} \left(P_{n-i} - PET_{n-i} \right), \; n \geq k$$

where k (months) is the timescale of the aggregation and n is the calculation number. The D values are undefined for $k > n$. Timescales from 1- to 24-months were used in this study. For example, to obtain the 6-month SPEI, first a time series is constructed by the sum of D values from five months before to the current month. Given the strong seasonal differences in the magnitude of P and PET and the climate regimes of each site, to obtain SPEI series comparable in space and time, it is necessary to transform the D series using equal probability to a normal distribution with a mean of zero and standard deviation of one so the values of the SPEI are really in standard deviations and lacks of seasonal effects. A log-logistic probability distribution function is fitted to the data series of D, as it adapts very well to all time scales. The complete calculation procedure for the SPEI can be found in Vicente-Serrano et al. (17).

At the shortest time scales (e.g. three months) there is a continuous alternation of short dry (negative SPEI values) and humid (positive SPEI values) periods (Figure S9). Highly plastic vegetation acclimated to this high frequency variability in moisture conditions in drought-prone areas and vegetation not so well adapted to withstand drought stress are expected to respond to these short-time droughts differently. At longer time scales (e.g., 12-24 months) droughts are less frequent and last more than at shorter scales. Vegetation well adapted to

withstand drought is also expected to respond to these time scales since it could be relatively insensitive to droughts acting at shorter time scales whereas persistent and sustained droughts acting at longer time scales might negatively affect plant communities from drought-prone areas.

The SPEI data has been obtained from the SPEIbase (45,S25), which is based on the CRU TS3.0 monthly precipitation and mean temperature dataset, compiled and processed by the Climate Research Unit of the University of East Anglia (http://badc.nerc.ac.uk/view/badc.nerc.ac.uk_ATOM_dataent_1256223773328276).

1.2. Assessment of the global aridity conditions

There are different indices proposed to assess the aridity of a region (S26-S28). All of these indices are based on values of precipitation and temperature or Potential Evapotranspiration (PET). The Environmental Programme of the United Nations (S29), proposed a drought index based on the quotient between precipitation and potential evapotranspiration. The quotient diminishes the role of the PET in relation to the precipitation on the aridity conditions. Then, to have an assessment of the global aridity we opted to calculate a simple climatic water balance based on the difference between the average annual precipitation and the average PET, which provides a quantification of the available deficit or surplus of water in each site. The PET was calculated according to the Thorthwaite equation (S27) since it only requires data of temperature to be calculated. Although the reference method accepted to estimate the PET by the Food and Agricultural Organization (FAO) is based on the Penmann-Monteith equation, it requires of several meteorological variables to be calculated (wind speed, solar radiation, relative humidity and temperature) which are not available at the global scale of the present study. Therefore, we opted for the use of the Thornthwaite equation (albeit slightly less accurate than other more complex approaches), given the low requirements of data and the general good results that it provides since it allows identifying the existing evapotranspiration differences at a global scale (Figure S10).

1.3. Quantifying vegetation activity from remote sensing images

At present the unique available empirical information at a global scale and the sufficient spatial resolution to identify differences between vegetation communities, mainly in areas of high spatial diversity in vegetation activity, is obtained from remote sensing images collected from earth observation satellites.

When the sun electromagnetic radiation reaches the plant leaves, a part of the energy is reflected and the rest is absorbed or transmitted. Nevertheless, the response of the active vegetation to the energy received at different longwaves is quite different. In the visible part of the electromagnetic spectrum there is a great energetic absorption due the vegetation pigments and to the energetic consumption by photosynthesis. On the contrary, in the region of the near infrared, most of the radiation is reflected as a consequence of the internal structure of the leaves (S30, S31).

It is possible to summarise the information received in the red and infrared regions of the spectrum by radiometers and to obtain a measure of the vegetation activity. This is commonly done by means of vegetation indices, which are combinations of spectral bands with the objective of emphasizing the photosynthetic active components (S32). Several vegetation indices have been developed (S33, S34). Nevertheless, at present the most extended and widely used index is the Normalized Difference Vegetation Index (NDVI) which is formulated as (S35):

$$NDVI = \frac{\rho_{NIR} - \rho_{red}}{\rho_{NIR} + \rho_{red}}$$

where ρ_{NIR} and ρ_{red} are the reflectance values of the near infrared and red bands, respectively. The NDVI has been shown to be highly correlated with vegetation parameters such as green leaf biomass and green leaf area (S36-S39) and it is an excellent proxy of the photosynthetic activity (S40,S41). The NDVI has also some limitations to analyse the dynamics of the vegetation activity because: i) the relationship between vegetation parameters (leaf area, ANPP, plant cover, etc.) and the NDVI are sometimes non-linear since the NDVI saturates before the maximum biomass is reached (S42,S43), ii) when canopy cover is sparse, there are substantial spectral background contributions (e.g. soil) to the overall remote sensing signal and iii) it is influenced by the amount of clear sky days and the level of atmospheric aerosols. Nevertheless, numerous authors have demonstrated the strong relationship existing between the NDVI and the leaf area index (S44) and the total vegetation biomass (S45-S48). Thus, recent studies have also shown that variations of the near infrared reflectance as a consequence of changes in the leaf water potential, which are associated with drought, are also observed in dense forests (S49). These findings indicate that even in these dense areas the NDVI can also record spectral variations associated with changes in vegetation activity related to drought. In addition, in dense forests of the Amazonian Basin, Brando et al. (40) have shown a significant association between the production of new leaves by trees and the values of the satellite-derived vegetation indices, which provides evidence on the sensibility of the vegetation spectral indices to changes in the tree activity and biomass of very dense forests. In any case, to provide more robustness to our results, we have also used improved vegetation indices obtained from recent satellite platforms that reduce the commented problems attributed to the NDVI (see below).

1.4. Vegetation activity datasets

Currently, there are several satellites recording land spectral information that allows quantifying the NDVI or

other vegetation indices. Among them, the unique satellites that record with a high temporal resolution global data are the NOAA, the SPOT-VEGETATION and the TERRA/AQUA satellites. The main problem of the satellite imagery recorded by these satellites is the short range of the available time series. The SPOT-VEGETATION data is available from the launching of the SPOT-VGT1 in 1998 and MODIS images are available from 2001. These periods are too short to obtain reliable conclusions about the drought impacts on vegetation activity. The longest time-series of satellite imagery at a global scale with the spectral bands that may obtain the NDVI are from the NOAA satellites since the first operative satellite with robust calibration was launched in 1981 (NOAA-7). Different NOAA satellites have been launched since 1981, but all of them have used the same sensor: the Advanced Very High Resolution Radiometer (AVHRR), which records information in the spectral band of the red and near infrared and allows calculating the NDVI (S50). In addition, the AVHRR data are recorded daily in any part of the world, which ensures availability of images with a high temporal frequency, independently of the cloud coverage.

Nevertheless, the precision of the NDVI time series obtained from NOAA-AVHRR images have problems related to the temporal homogeneity and stability of the NOAA satellites (S51) since the satellite changes and the orbit degradations may affect noticeably the derived NDVI products (S52).

Given the great applicability of the available NOAA-AVHRR images, different research and earth observation organisms have devoted a great effort to create long-term homogeneous NDVI datasets at a global scale and at the spatial resolution of the AVHRR Global Area Coverage, i.e. a grid size of 8 x 8 km. A review of the available datasets has been recently published (S53). Among the existing datasets, we have selected the NOAA Global Inventory Modeling and Mapping Studies (GIMMS) Normalized Difference Vegetation Index (NDVI) (46) since it covers a longer period than the other existing datasets (1981-2006). The NOAA GIMMS NDVI data were generated from the original 1.1 km^2 NOAA AVHRR data as bi-weekly maximum value composites aggregated to an 8 x 8 km pixel resolution. The quality and consistency of the GIMMS data were assured by the correction for i) sensor degradation, ii) sensor inter-calibration differences, iii) solar zenith and viewing angles, iv) volcanic aerosols, v) atmospheric water vapour and vi) cloud cover. By comparing NOAA GIMMS and Landsat images, Beck et al. (S53) have shown that the GIMMS is the most accurate AVHRR-NDVI dataset for assessing vegetation variability and trends.

The new MODIS sensor on board of the satellites AQUA and TERRA shows improved capabilities regarding previous satellite platforms (S54). The higher number of spectral bands of the MODIS sensor in comparison to the AVHRR allows calculating additional vegetation indices. Among them, the Enhanced Vegetation Index (EVI) (S55, S56) was developed to optimize the vegetation signal with improved sensitivity in high biomass regions and enhanced vegetation monitoring and a reduction in atmosphere influences. The EVI has been widely used in the last years since it is more responsive to canopy structural variations, including leaf area index (LAI), canopy type, plant physiognomy, and canopy architecture than NDVI (S56). For this reason, although the MODIS data encompass a much shorter period of data as compared with the GIMMS-NDVI dataset since the former has only 9 years of common data with the SPEIbase (2001-2009), we have also included the EVI and NDVI datasets from the MODIS Collection 5 (C5) in the analyses (S57).

1.5. Tree-ring growth data

We compiled 1846 tree-ring width chronologies encompassing the period 1945-2009 archived by the National Climate Data Center (NCDC) in the the International Tree-Ring Data Bank (ITRDB) (S58). These annually resolved archives are kindly provided by dendrochronologists and are available online at: http://www.ncdc.noaa.gov/paleo/treering.html. Each chronology represents the average radial growth series of several trees (typically more than ten) of the same species growing in the same site. The wood samples are taken following standard protocols which include sampling at least ten trees within a local population, taking usually two radial cores per tree at 1.3 m. The selected 1846 sites corresponded to those chronologies listed in the ITRDB in November 2011 with at least ten trees sampled after 1940, which we regarded as an acceptable criterion for robust replication within each site. Most sites with tree-ring width data available at the ITRDB were located in North America and Europe (Figure S11).

Wood samples are air-dried and polished using sand-papers of progressively finer grain or transversally sectioned until tree-rings are clearly visible under a binocular. Then, they are visually cross-dated using characteristic rings (S59). The ring widths of cross-dated samples are measured using semi-automatic devices usually with a resolution of 0.01 mm. Then, the visual cross-dating of measured samples is checked with the COFECHA program which calculates correlations between the individual series measured for each radius and the mean average series considering fixed time intervals (S60). All conversions among the different formats used by the dendrochronological community were done using the TriCycle program to obtain decadal files (S61).

Raw ring-width measurements were standardized to remove long term biological growth trends associated with tree ageing and increasing trunk diameter, but to preserve interannual and interdecadal variability, often associated with climate variability including changes in SPEI (11). Standardizations were carried out by the original scientists who contributed the chronologies to the ITRDB (see a similar analysis in S62). Usually, individual series of tree-ring widths were fitted with negative exponential curves or linear functions and

residuals were obtained by dividing the observed by the fitted values. The resulting width residuals were subjected to autorregressive modelling and then averaged for each year using a biweight robust mean to obtain a mean residual chronology of prewhitened growth indices for each site. The detrending procedure was performed using the program ARSTAN (S63). In the case of long chronologies (length > 300 years) corresponding to forests with old trees, trends in ring-width indices for the late 20th century were further removed by fitting linear regressions and keeping the resulting residuals.

1.6. Methods

The procedure followed to calculate the correlations between the SPEI series and the series of the three vegetation parameters is illustrated in Figure S12. It corresponds to the GIMMS-NDVI in a warm temperate thorn scrub in South Africa (25.9ºE, 25.9ºS). It shows the evolution of the March standardized NDVI and the March series of SPEI at the time scales of 1, 3 and 12 months and it is clear that there is a close agreement between the NDVI and the 3-month SPEI. Thus, considering all the SPEI time scales, from 1 to 24 months, maximum correlation is recorded at the 3-month time scale, which means that the magnitude of the NDVI in March is mostly determined by the cumulative water balance occurring from January to March. Therefore, both, the maximum correlation recorded (0.68) and the 3-month time-scale are retained for further analysis. The same approach is applied to the tree-ring growth and ANPP, but given that the series are annual, they are correlated with the 1- to 24-month SPEI series of each month of the year, identifying the month of the year and the SPEI time scale at which maximum correlation is reach, and the magnitude of the maximum correlation.

We obtained monthly maps of relationships between GIMMS and MODIS vegetation indices and different time scales of the SPEI (Figure S13). The maps A to D represent the correlations found between the time series of May GIMMS-NDVI and that of May SPEI at the time scales of A) 3, B) 6, C) 12 and D) 18 months. The figures show similarities and differences in the spatial patterns and magnitude of correlations. The plot E) shows the maximum correlation for May between the SPEI and the GIMMS-NDVI, which is a composite map created from the correlations indicated in the maps A) to D) and also including other SPEI time scales (from 1 to 24 months). The plot E) shows the maximum correlation found between NDVI and SPEI at time scales ranging from 1 to 24 months. The plot F) represents the SPEI time scale at which the maximum correlations are found. The seasonal and annual maps were created by the maximum of the corresponding monthly correlation maps.

The influence of droughts on tree growth and ANPP was also assessed by means of the Pearson coefficient computed between the annual ANPP and tree-ring width series and the 1- to 24-month monthly SPEI series of the 0.5º grid that included the corresponding forest and ANPP sites. Therefore, for each tree-ring width series we also obtained 288 correlations. Maximum correlations and corresponding time scales were mapped and retained for further analyses. Since both low- to mid-frequency variability and the first-order autocorrelation were removed in the residual tree-ring series of prewhitened width indices to avoid the decreasing trend of tree-ring width as trees enlarge and age, the 1- to 24-month SPEI series were also detrended for the period of available tree-ring data between 1945 and 2006 before calculating correlations.

2. Supplemental Seasonal Analysis

Analyses on the SPEI time scales at which maximum correlations between the SPEI and the GIMMS-NDVI were observed are also provided seasonally (Figure S14) to identify the existing seasonal differences as a consequence of the vegetation phenology in the global vegetation. The relationship between the annual water balance across eco-regions versus the SPEI/GIMMS-NDVI maximum correlations (Figure S15) and the corresponding time scales at which these maximum correlations are found (Figure S16) are also shown. These figures clearly show small differences among seasons and a similar pattern to that shown at an annual scale.

3. Supplemental analysis of MODIS images

To strength the robustness of the obtained results with the GIMMS-NDVI dataset, analysis have been performed using EVI and NDVI data from the MODIS images between 2001 and 2009. The results show similar results to those indicated with the GIMMS-NDVI, both for the annual and seasonal analyses. The spatial distribution of the maximum annual correlations between SPEI and MODIS-EVI and –NDVI are shown in Figure S17. The seasonal maximum correlations are shown for the EVI and the NDVI in Figures S18 and S19, respectively. Areas with statistically significant correlations are shown in Figures S20 and S21 for EVI and NDVI datasets, respectively. The relationship between the SPEI/EVI and NDVI maximum correlations and the annual water balance across eco-regions is shown in Figure S22. The SPEI time scales at which maximum correlations between the SPEI and the MODIS EVI and NDVI are found are shown annually (Figure S23) and seasonally (Figures S24 and S25).

4. Supplemental Figures and Tables

Site	latitude	longitude	years of data	Type of vegetation	Source
Hopland field station	38.96	-123.1	16	Pasture	(S64)
Carey Kipuka	43.33	-113.53	10	Pasture	(S65)
Little Crater	42.87	-113.13	10	Pasture	(S65)
Hansel Valley	41.68	-112.58	10	Pasture	(S65)
Rattelsnake pass	41.86	-112.5	10	Pasture	(S65)
Morgan Pasture	43.45	-112.47	10	Pasture	(S65)
Kettle Butte	43.54	-112.43	10	Pasture	(S65)
Benmore	40.03	-112.4	11	Pasture	(S66)
Snake river plain	44.3	-112.3	13	Grasses and shrubs	(S67)
Manyberries	49.4	-110.68	50	Pasture	(S68)
Santa Rita	31.85	-110.57	10	Pasture	(S69)
Doña Ana	32.53	-106.86	32	Pasture	(S70)
Jornada	32.6	-106.7	19	Black grama grassland	(2)
Sevilleta	34.3	-106.6	10	Mixed desert grassland	(2)
Niwot Ridge	40.1	-105.6	15	Moist alpine meadow	(2)
Cheyenne	41.18	-104.88	17	Grassland	(S71)
Central Plains Experimental range	40.83	-104.7	50	Grassland steppe	(S72)
Sidney (Montana)	47.7	-104.15	12	Pasture	(S73)
Great Plains Field Station	46.81	-100.88	16	Pasture	(S74)
Missouri	46.76	-99.46	21	Pasture	(S75)
Hays	38.86	-99.31	24	Pasture	(S76)
Montecillo	19.46	-98.91	10	Saline Grassland	(S77)
Flint Hills	39.18	-96.58	42	Pasture	(S78)
East Bay Ballou	29.6	-94.41	13	Grasses	(S79)
Cedar Creek	45.4	-93.2	23	Oak savanna grassland	(2)
Kellogs	42.4	-85.4	10	Successional field	(2)
Barro Colorado	9.15	-79.85	11	Tropical forest	(S77)
Debordieu	33.33	-79.25	10	Wet forest	(S80)
Harvard Forest	42.48	-72.18	18	Mixed deciduous Forest	(2)
Hubbord Brook	43.9	-71.71	10	Mixed deciduous Forest	(2)
Patagonia Argentina	-45.68	-70.26	10	Pasture	(S81)
Sydenham	-29.1	27.25	19	Pasture	(S82)
Towoomba	-24.9	28.35	19	Fine-leaved savanna	(S77)
Migda	31.36	34.42	10	Pasture	(S83)
Yaakov	33.01	35.25	13	Pasture	(S84)
Kursk	51.67	36.5	29	Meadow steppe	(S77)
Dzhanybek	49.33	46.78	33	Semi-desert steppe	(S77)
Badkhyz	35.68	62	31	Desert steppe	(S77)
Xilin	43.63	116.7	24	Steppe	(S85)
San Joaquín	37.08	119.76	13	Pasture	(S86)
Tumugi	46.1	123	10	meadow steppe	(S77)
Paracou*	5	-52.08	11	Tropical forest	(S87)
Boukoko*	3.25	18	13	Tropical forest	(S87)
Sungei Menyala Forest Reserve*	2.46	101.91	13	Tropical forest	(S88)

Table S1. Series of Aboveground Net Primary Production (ANPP) used in this study. The location, years of data, type of vegetation and data sources are also included. Raw data was obtained from published tabular data or by digitizing figures. Positive and negative values for latitude and longitude correspond to N or S and E or W hemispheres, respectively. Given the difficulty of estimating ANPP in forest sites (S89), forest areas are underrepresented, mainly in tropical and equatorial areas. To limit this problem and given the close relationship found between annual stem wood production and ANPP (S90,S91), we have also included three time series of growth increments obtained in tropical forests. Series marked by * correspond to series of annual stem growth increments based on repeated measures of diameter at 1.3 m. Annual ANPP data published in the different studies is commonly obtained in the periods of peak biomass. In the case in which monthly data is published, we have selected the monthly series corresponding to the peak of vegetation biomass.

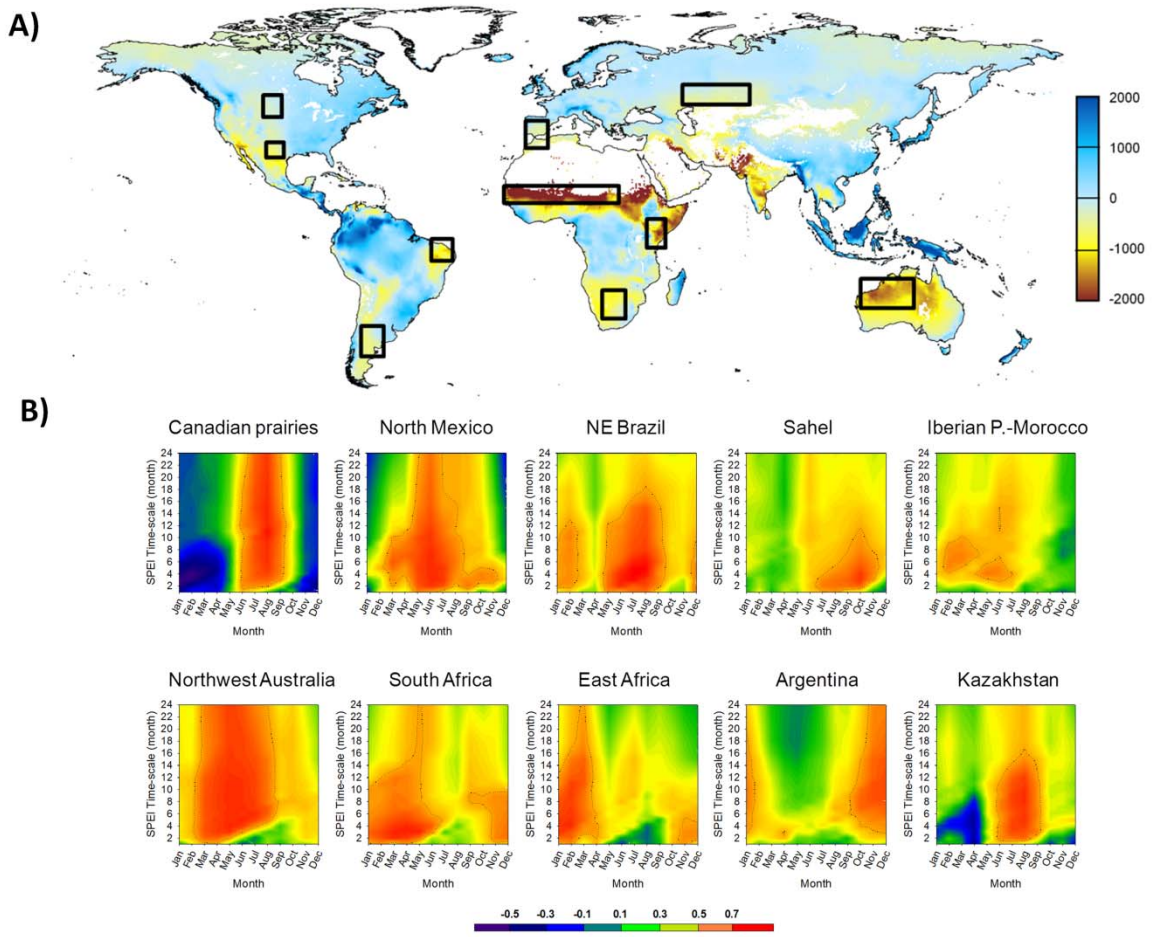

Figure S1. A) Average annual water balance (difference between annual precipitation and potential evapotranspiration in mm) for the period 1976-2006. Deserts are masked in white. **B)** Correlations (Pearson coefficient) between the SPEI at time scales from 1 to and 24 months and the GIMMS-NDVI in different regions of the world (see the map in A) for the period 1981-2006. Dotted lines frame statistically significant correlations ($\alpha < 0.05$). In the Canadian prairies drought determines, to a large extent, vegetation activity during the boreal summer, and the vegetation response seems to be insensitive to the drought time scale. However, in other areas (e.g. Argentina) the influence of drought is greatest at long time scales (> 8 months), while in the Sahel its effect mostly occurs at short ones (< 6 months). In some areas the vegetation response to drought can be more complex, even bimodal (e.g. NE Brazil and the Iberian Peninsula), as it can act at long and short time scales in seasonally specific responses.

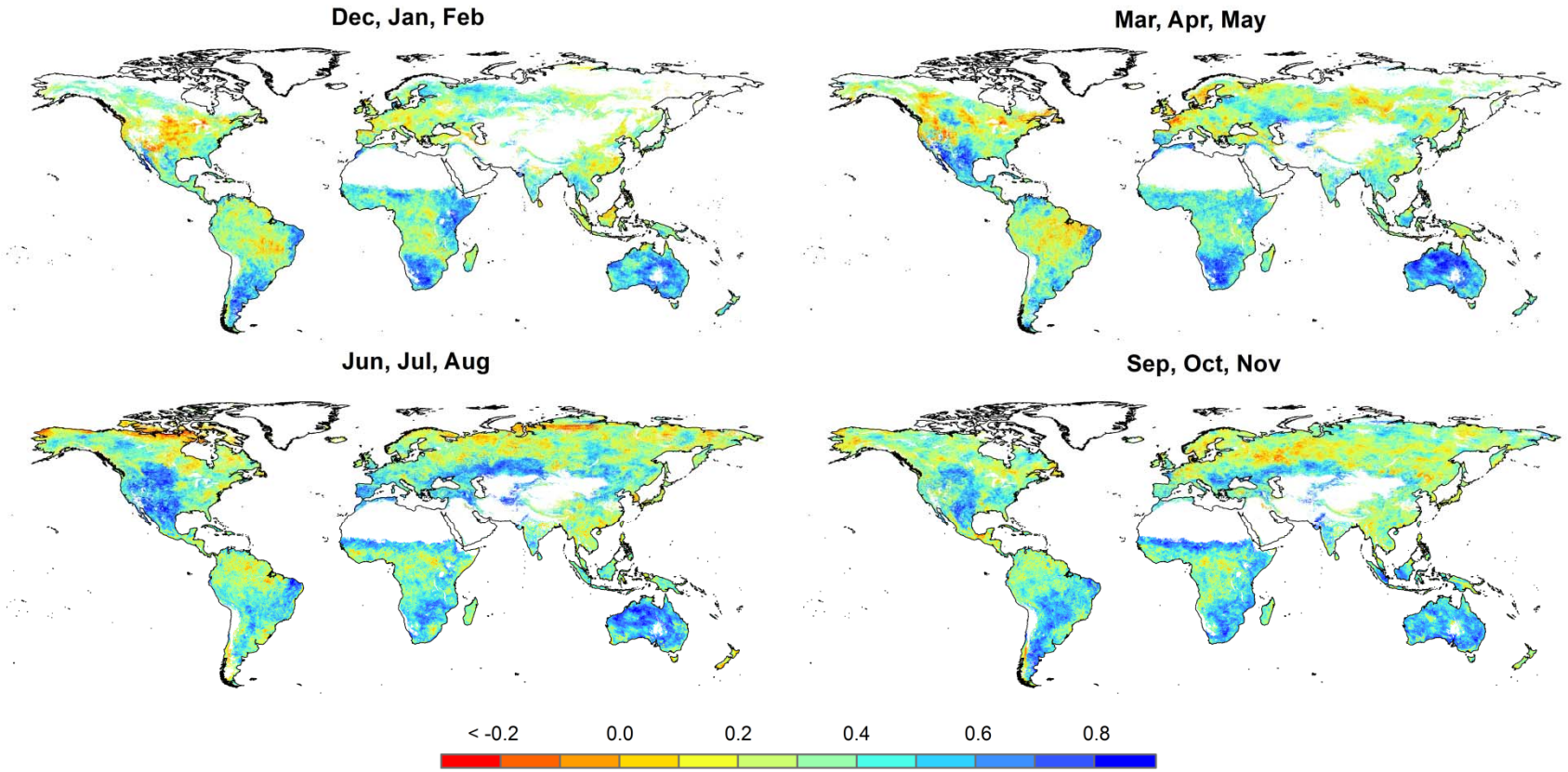

Figure S2. Spatial distribution of the seasonal correlations (Pearson coefficient) between SPEI and GIMMS-NDVI for the period 1981-2006. The values represent the maximum correlation (*r*) recorded for each pixel, independently of the month and the SPEI time scale. Desert and ice areas are masked and not included in the analysis.

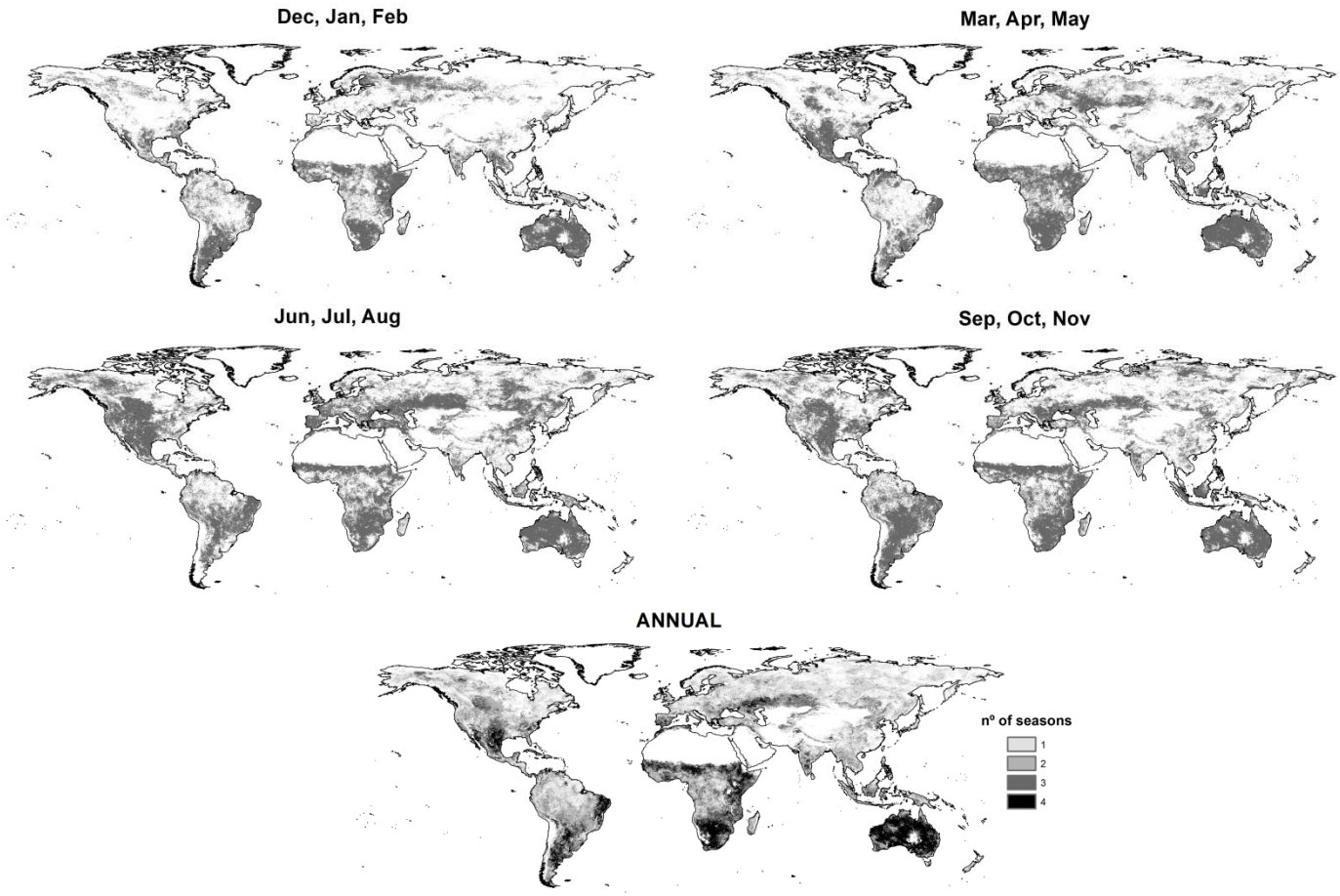

Figure S3. Areas with statistically significant Pearson correlation coefficients ($\alpha < 0.05$) between the SPEI and the GIMMS-NDVI calculated at seasonal and annual resolutions. The legend of the lowermost annual map indicates the number of seasons in which significant correlations were obtained.

Season	Surface (x 10^6 km^2)	% Total world	% vegetated areas
Dec.,Jan.,Feb.	97.53	23.60	43.92
Mar.,Apr.,May	113.28	28.38	45.47
Jun.,Jul.,Aug.	138.84	36.70	47.98
Sep.,Oct.,Nov.	133.55	35.16	47.80
Annual	218.40	57.50	72.00

Table S2. Surface of the world with significant Pearson correlation coefficients ($\alpha < 0.05$, $r > 0.38$) between the SPEI and the GIMMS-NDVI (1981-2006). The vegetated areas were obtained from the GlobCover dataset.

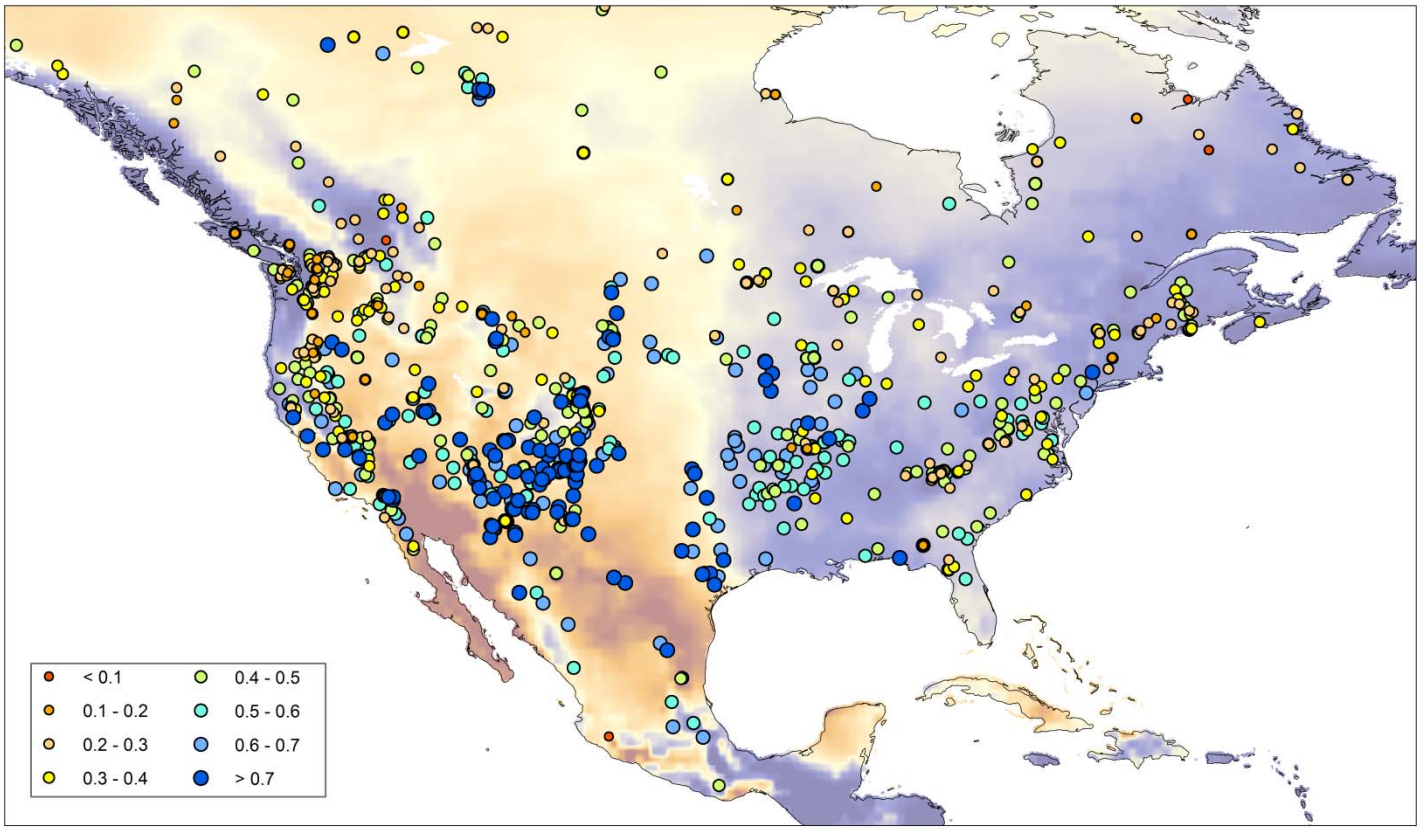

Figure S4. Spatial distribution of the correlations (Pearson coefficients, *r*) between SPEI and tree-ring width series for the period 1945-2009 in North America. The values represent the maximum correlation recorded for each pixel, independently of the month of the year and the SPEI time scale. The background colours represent the distribution of the water balance indicated in Figure S1.A.

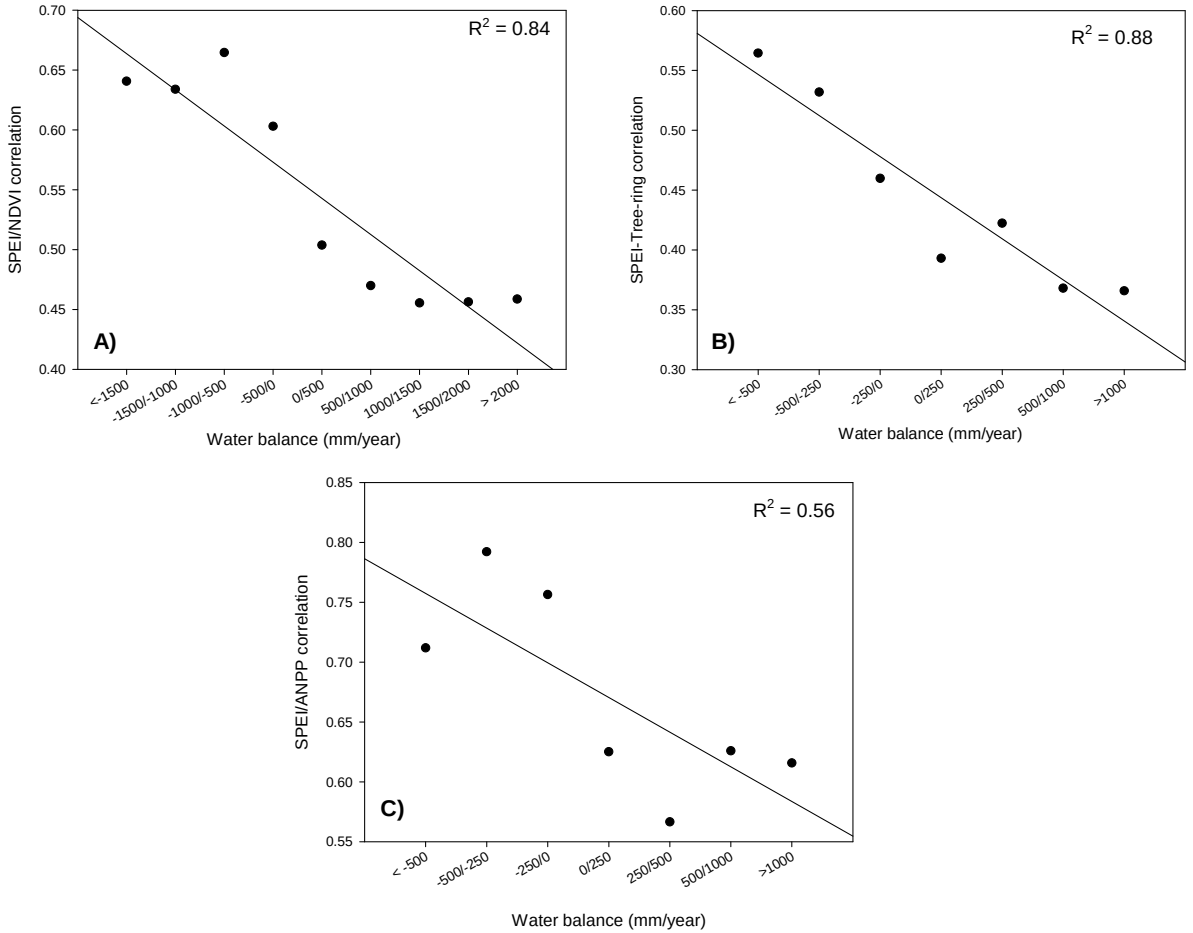

Figure S5. (A) Average values of the GIMMS-NDVI/SPEI maximum correlations summarized for different ranges of the annual water balance (precipitation minus PET), **(B)** Average values of the tree-ring width/SPEI maximum correlations summarized for different ranges of the annual water balance. **(C)** Average values of the ANPP/SPEI maximum correlations summarized for different ranges of the annual water balance. Results of the linear fitting by means of the coefficient of determination are also shown.

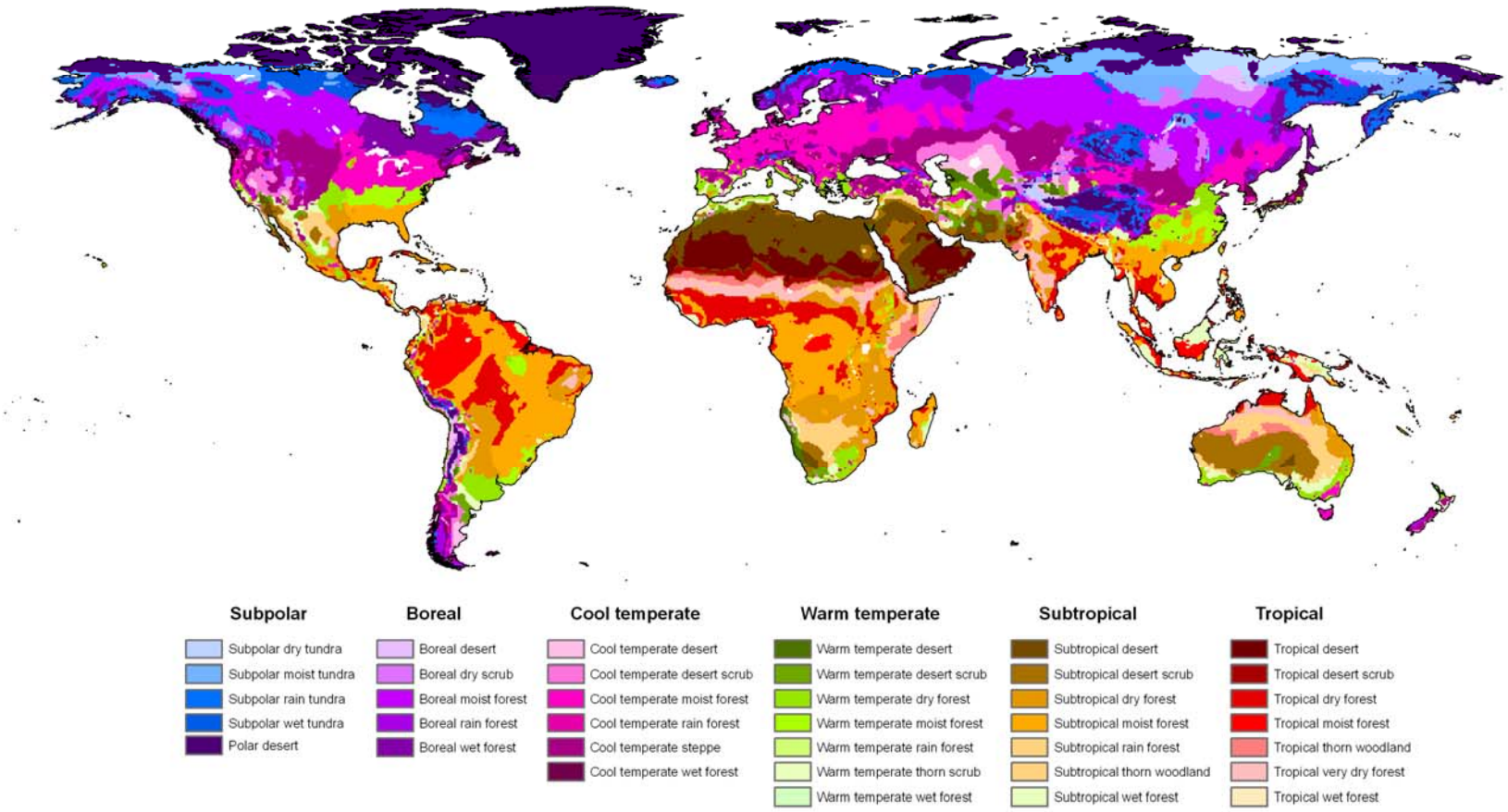

Figure S6. Map of the Holdridge classification system of eco-regions and biomes (48).

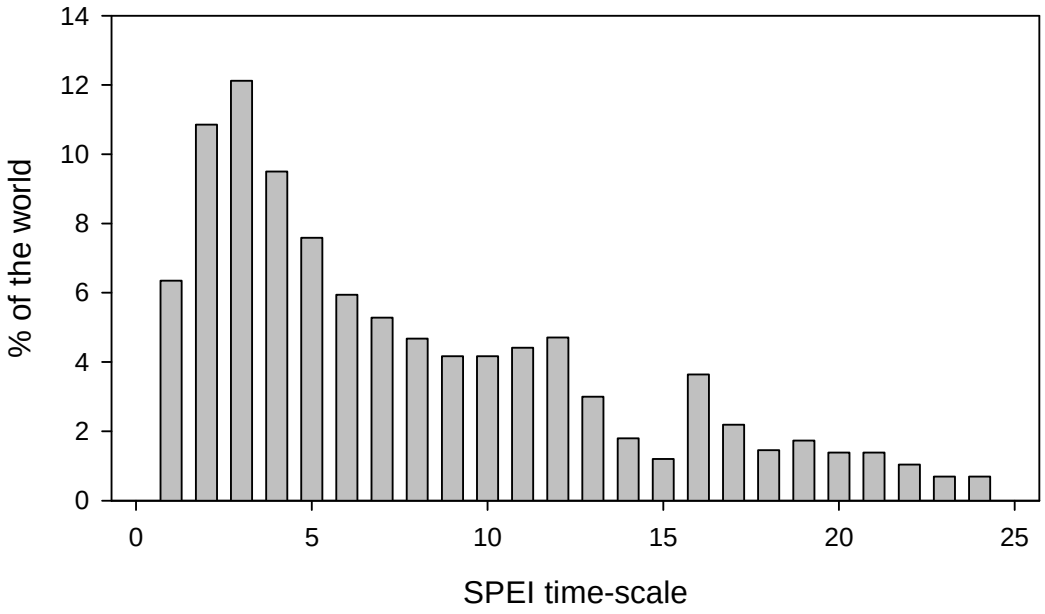

Figure S7. Percentage of the world terrestrial area covered by vegetation in which maximum GIMMS-NDVI/SPEI correlations are found at different SPEI time scales (in months).

A)

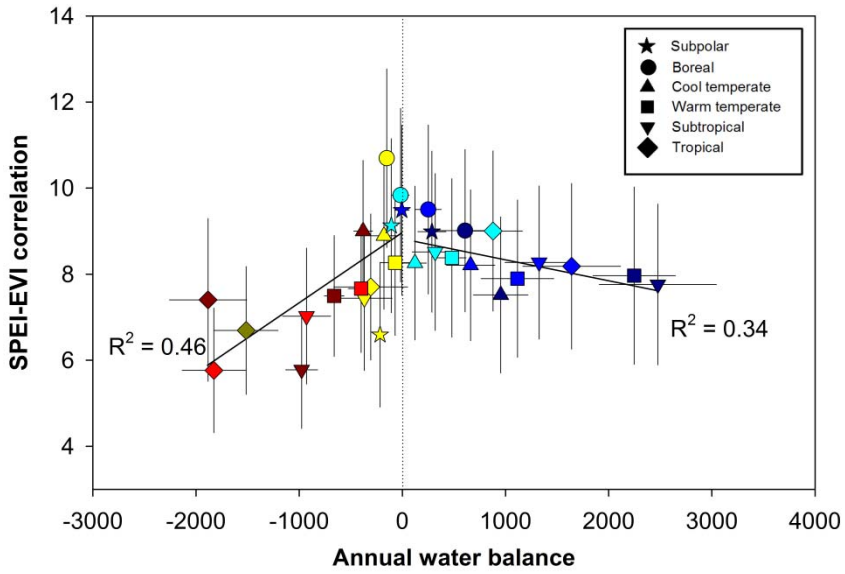

B)

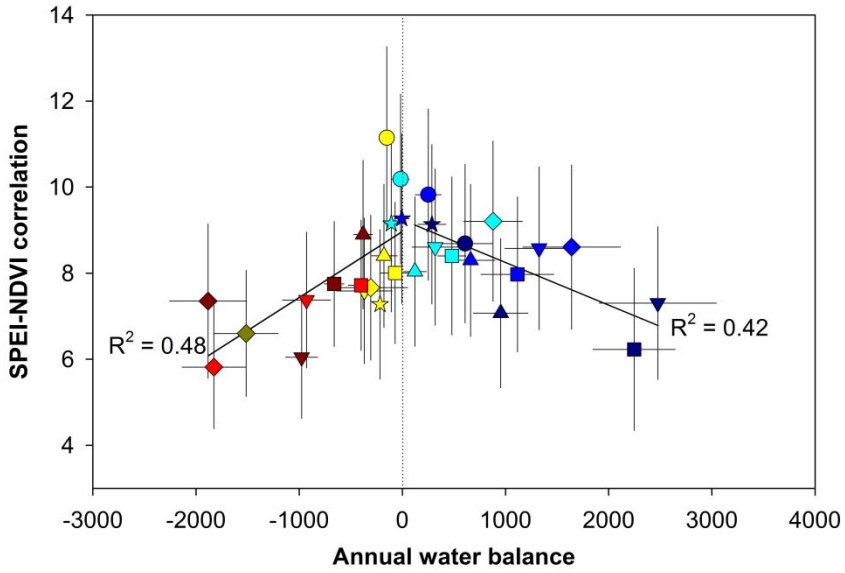

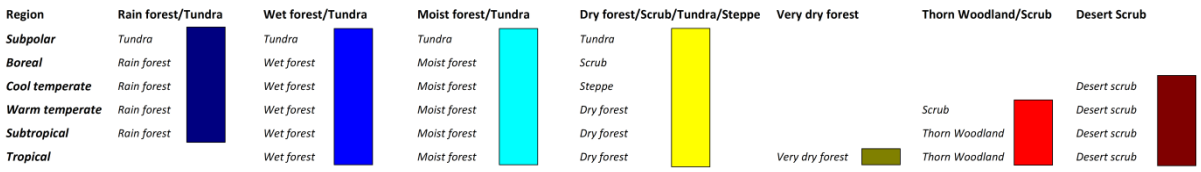

Figure S8. Relationship between the average SPEI time scales at which the maximum SPEI/MODIS **A)** –EVI and **B)** -NDVI correlation is found and the average annual water balance across eco-regions. The biomes are grouped according to the six existing eco-regions: Subpolar, Boreal, Cool temperate, Warm temperate, Subtropical and Tropical. Colors represent the different biomes of each one of the six eco-regions in the A and B plots and the symbols represent the different eco-regions.Results of the linear fitting by means of the coefficient of determination are also shown. Error bars represent ± ½ standard deviations.

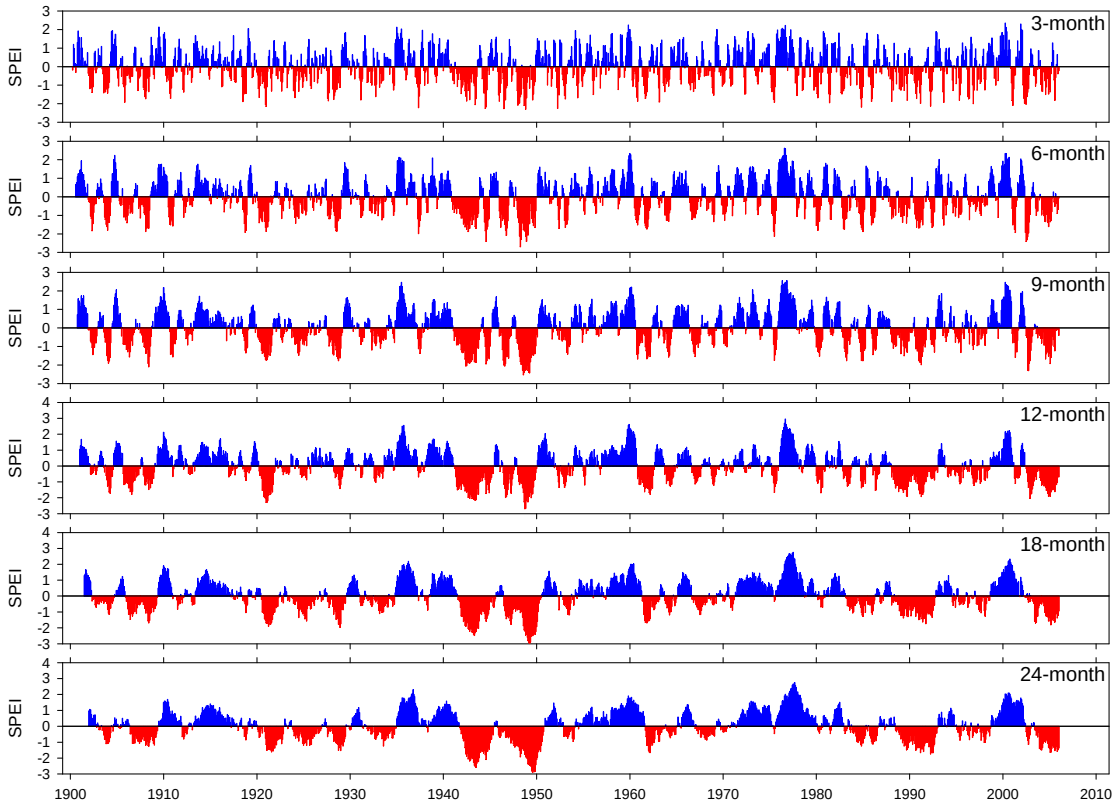

Figure S9. Example of drought evolution on different time scales as assessed by the SPEI. The series represents the evolution of the SPEI at 46.5°N, 8°E. Dry (negative SPEI values) and humid (positive SPEI values) periods are represented by red and blue bars, respectively.

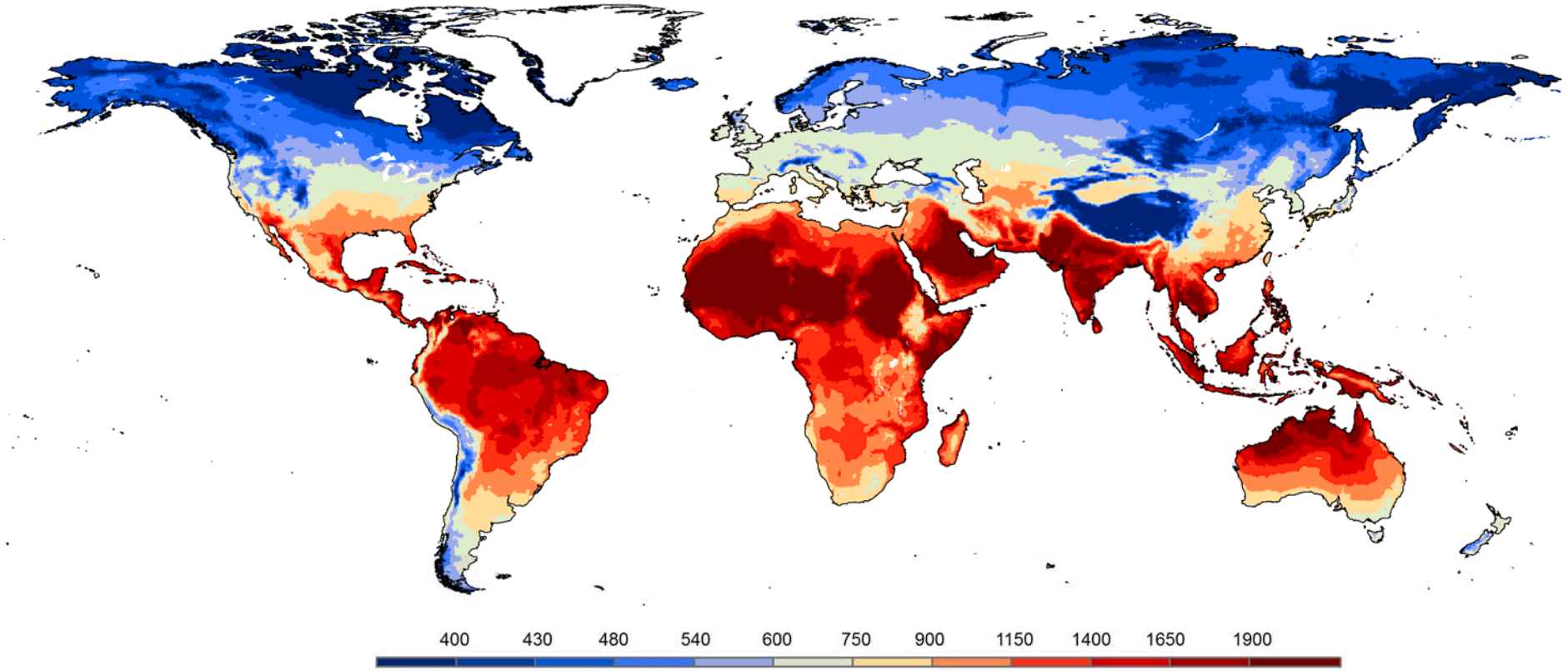

Figure S10. Spatial distribution of the average (1970-2000) potential evapotranspiration (PET) following the Thornthwaite's method.

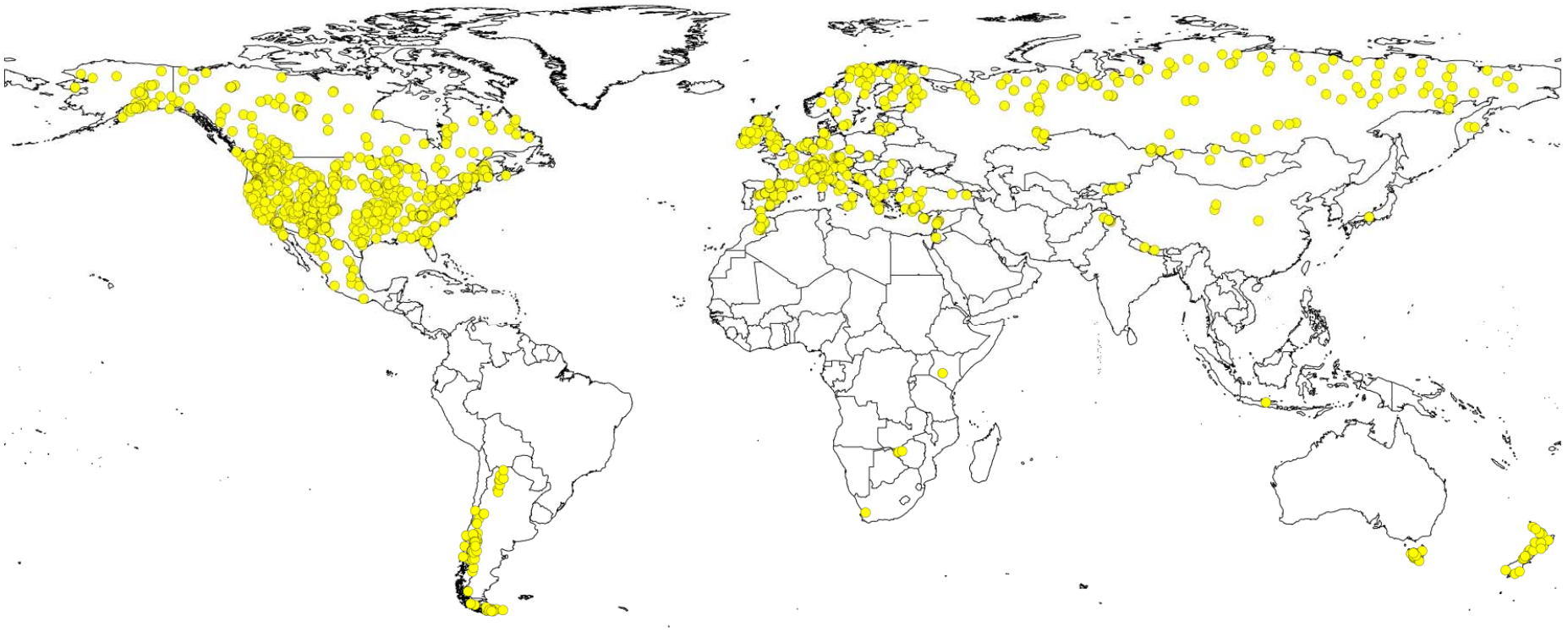

Figure S11. Spatial distribution of the tree-ring width series used in this study

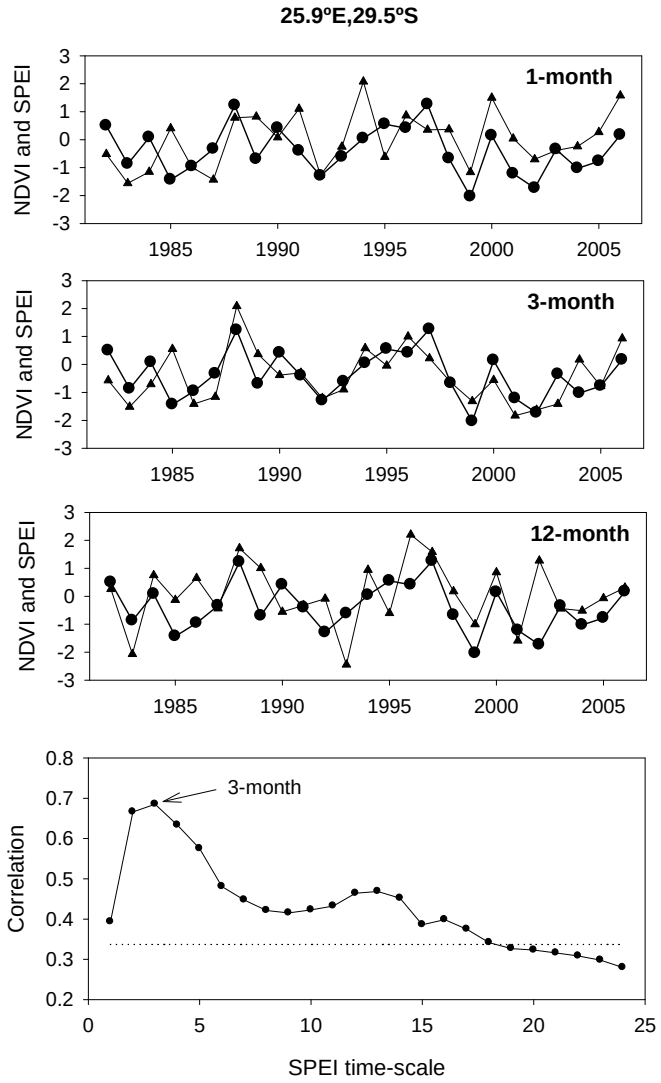

Figure S12: Evolution of standardized GIMMS-NDVI and 1-, 3- and 12-month SPEI in March in a warm temperate thorn scrub in South Africa (25.9ºE, 25.9ºS). The correlation between the NDVI (circles) series and the 1- to 24-SPEI (triangles) timescales is shown in the lower panel. Dotted line shows the threshold for statistically significant correlations.

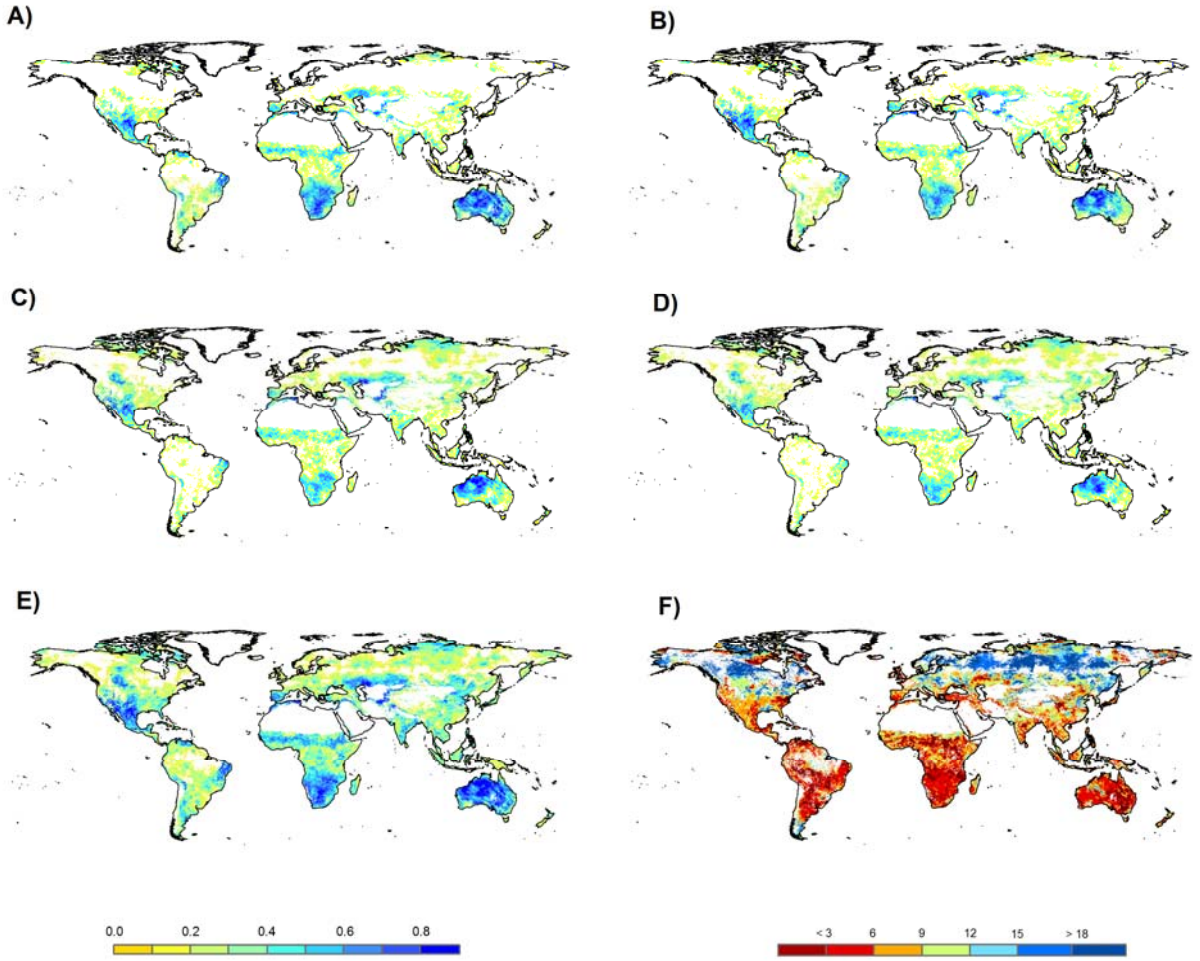

Figure S13. Spatial distribution of the May GIMMS-NDVI/SPEI correlations at the time scales of **A)** 3-, **B)** 6-, **C)** 12- and **D)** 18-months; **E)** maximum correlation found at time scales from 1 to 24 months and **F)** SPEI time scale (in months) at which the maximum correlation is found.

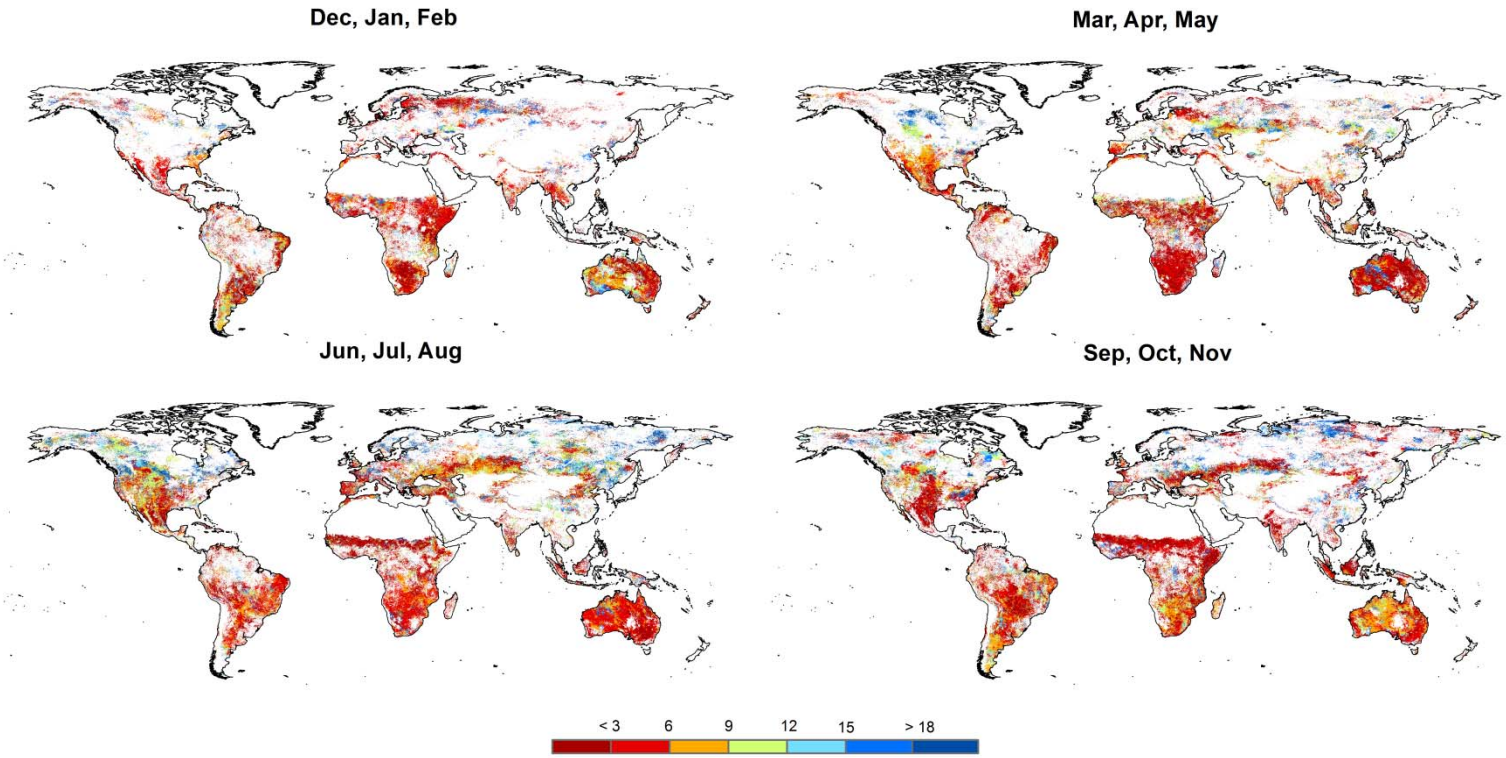

Figure S14. SPEI time scale (in months) at which the maximum seasonal correlation between SPEI and GIMMS-NDVI is found. Areas with no significant correlations are depicted in white. Desert and ice areas are masked and not included in the analysis.

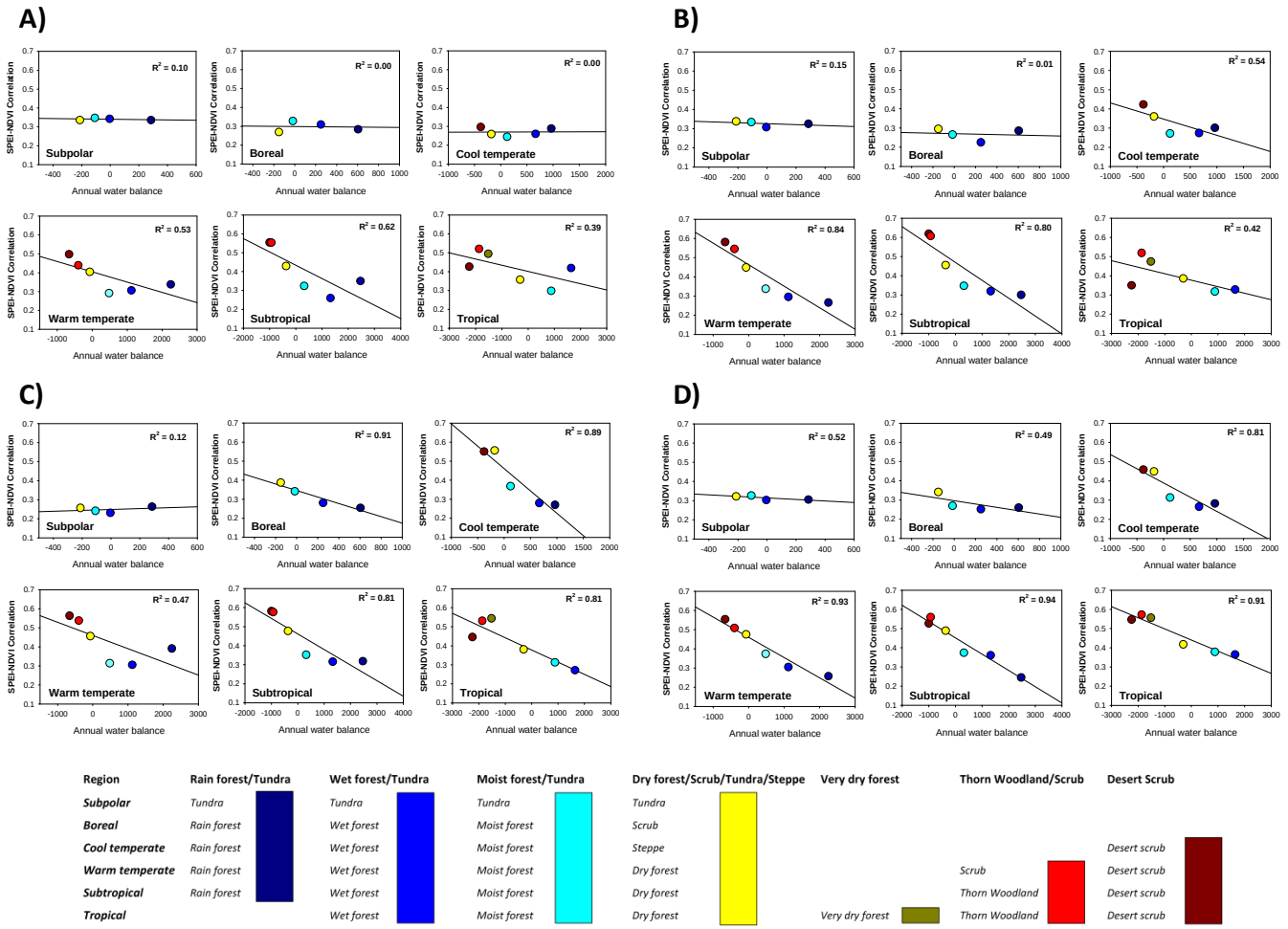

Figure S15. Relationships between SPEI/GIMMS-NDVI maximum Pearson correlation coefficients and the annual water balance across eco-regions. **A)** Dec, Jan, Feb; **B)** Mar, Apr, May; **C)** Jun, Jul, Aug; **D)** Sep, Oct, Nov. The biomes are grouped according to six eco-regions: Subpolar, Boreal, Cool temperate, Warm temperate, Subtropical and Tropical. All the biomes are represented by the same symbol (circle).

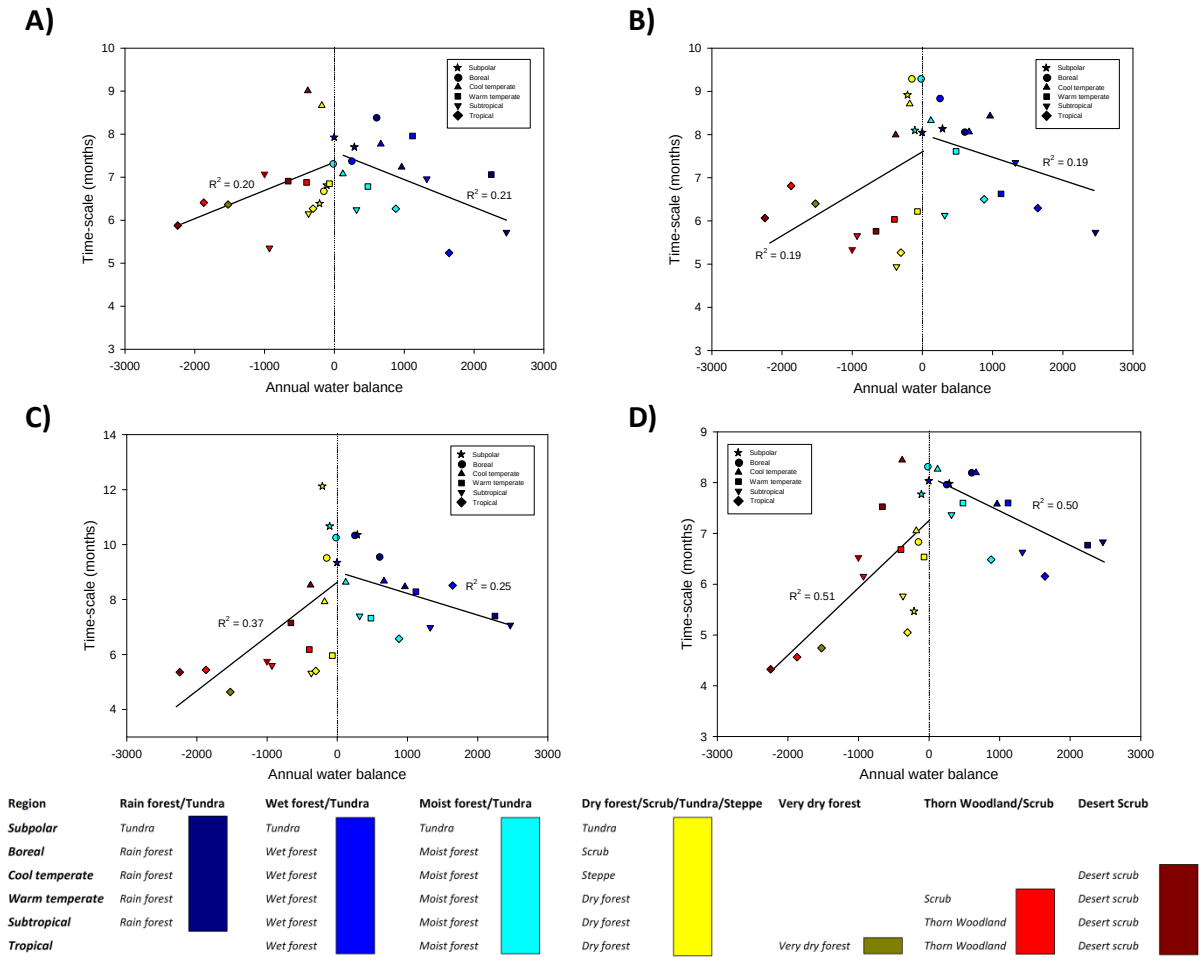

Figure S16. Seasonal relationships between the average SPEI time scales at which the maximum SPEI/GIMMS-NDVI correlation is found and the average annual water balance across eco-regions. **A)** Dec, Jan, Feb; **B)** Mar, Apr, May; **C)** Jun, Jul, Aug; **D)** Sep, Oct, Nov. The biomes are grouped according to the six existing eco-regions: Subpolar, Boreal, Cool temperate, Warm temperate, Subtropical and Tropical. Colors represent the different biomes of each one of the six eco-regions in the four plots and the symbols represent the different eco-regions.

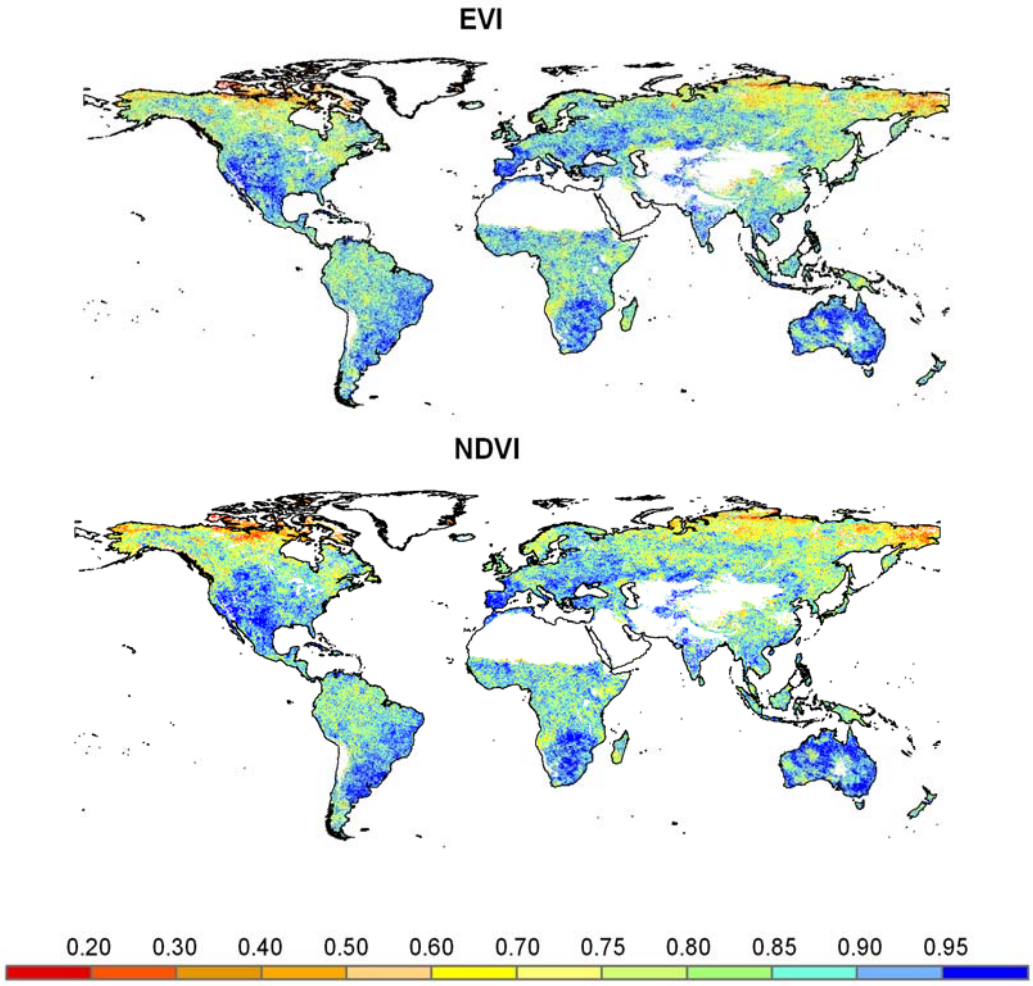

Figure S17. Spatial distribution of the correlations (Pearson coefficient, *r*) between SPEI and MODIS-EVI AND -NDVI for the period 2001-2009. The values represent the maximum correlation recorded for each pixel, independently of the month of the year and the SPEI time scale. Desert and ice areas are masked and not included in the analyses.

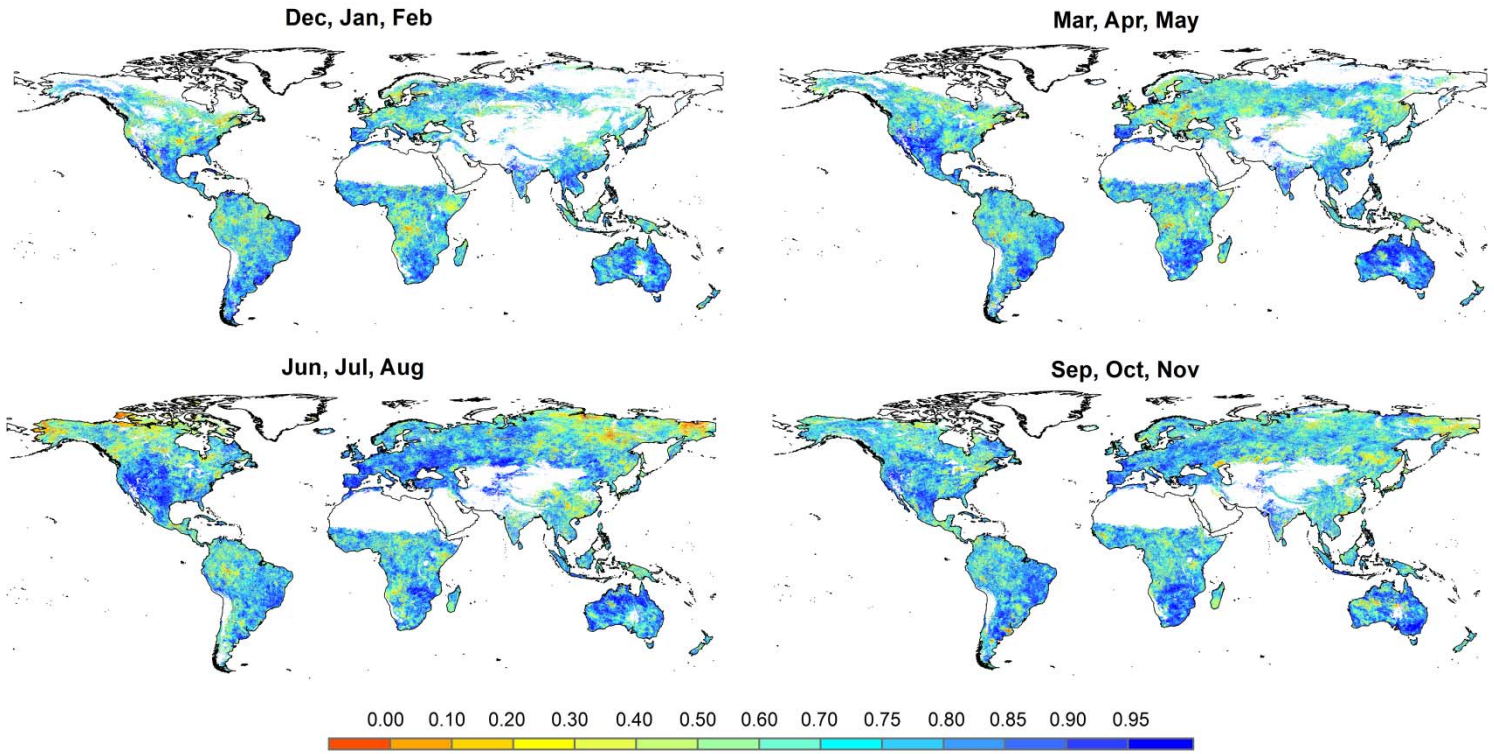

Figure S18. Spatial distribution of the seasonal correlations (Pearson coefficient, *r*) between SPEI and MODIS-EVI for the period 2001-2009. The values represent the maximum correlation recorded for each pixel, independently of the month of the year and the SPEI time scale. Desert and ice areas are masked and not included in the analysis.

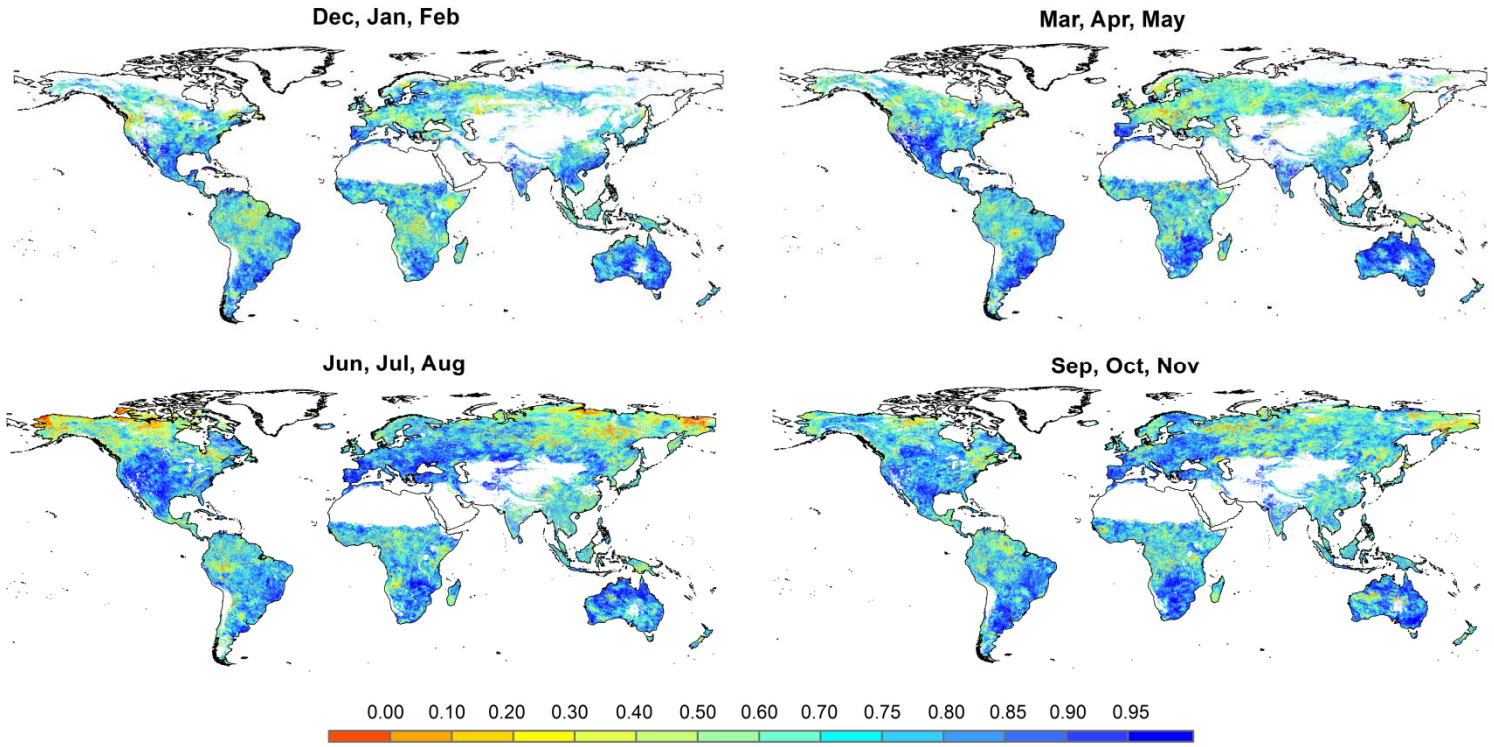

Figure S19. Spatial distribution of the seasonal correlations (Pearson coefficient, *r*) between SPEI and MODIS-NDVI for the period 2001-2009. The values represent the maximum correlation recorded for each pixel, independently of the month of the year and the SPEI time scale. Desert and ice areas are masked and not included in the analysis.

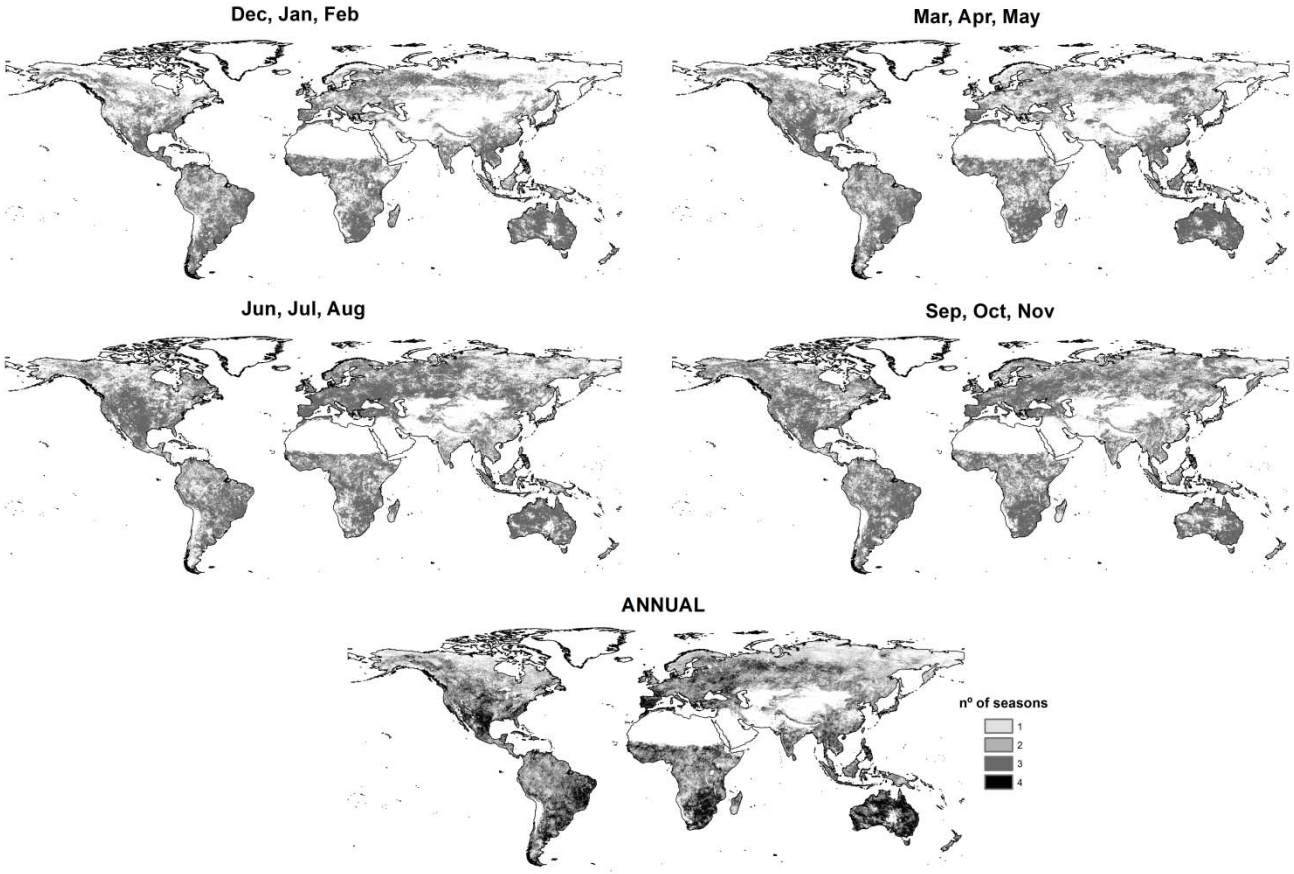

Figure S20. Areas with statistically significant Pearson correlation coefficients ($\alpha < 0.05$) between the SPEI and the MODIS-EVI for each season and the whole year. The legend of the lowermost annual map indicates the number of seasons in which significant correlations were obtained.

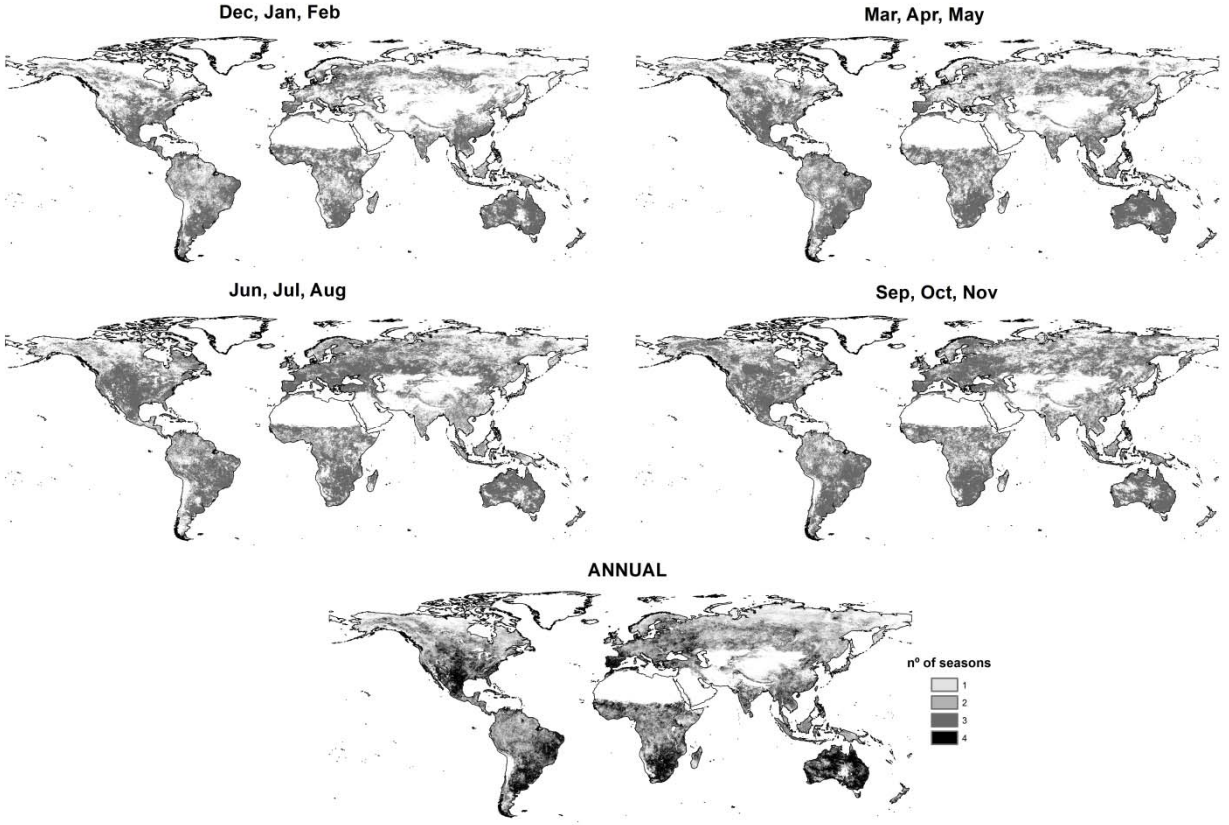

Figure S21. Areas with statistically significant Pearson correlation coefficients ($\alpha < 0.05$) between the SPEI and the MODIS-NDVI for each season and the whole year. The legend of the lowermost annual map indicates the number of seasons in which significant correlations were obtained.

A)

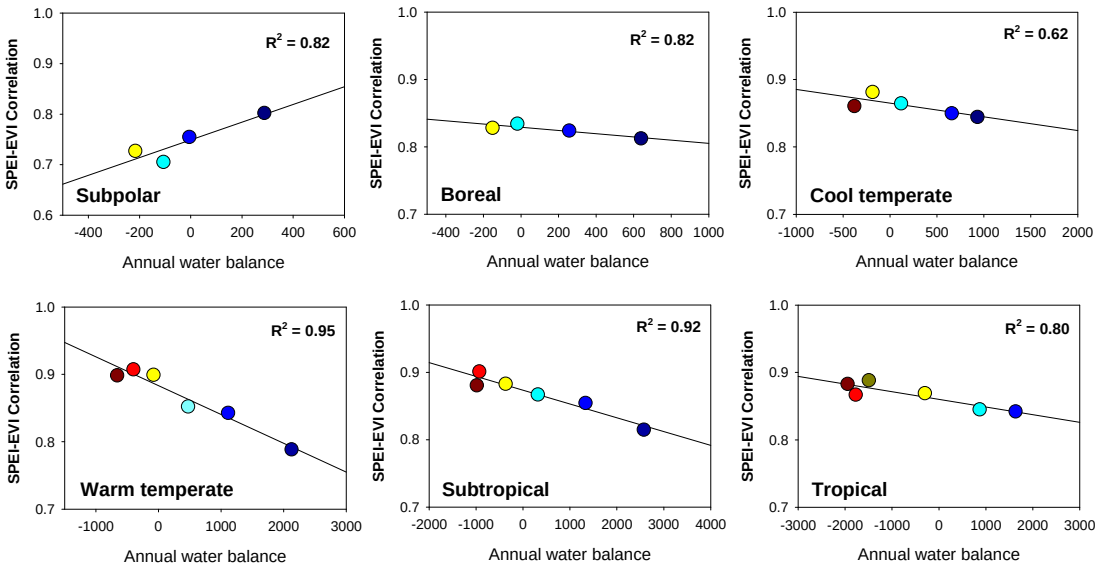

B)

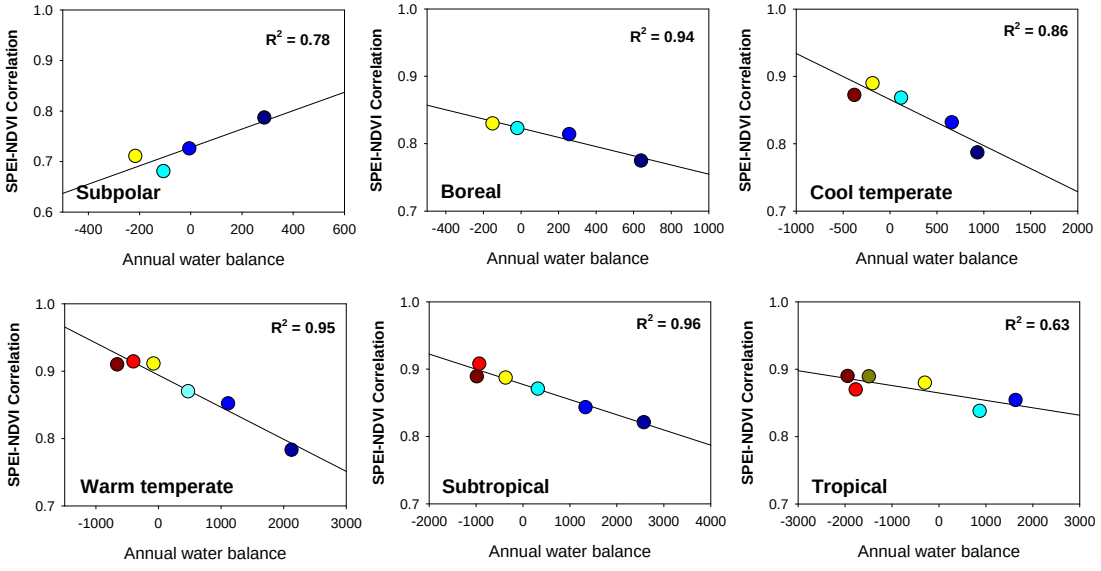

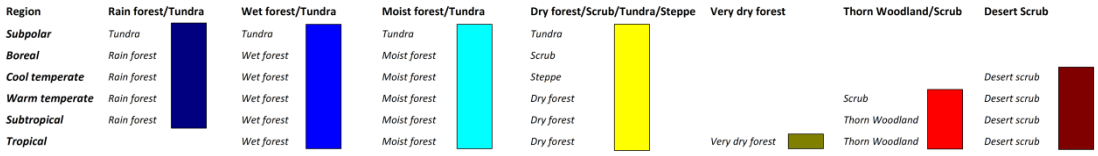

Figure S22. Relationship between **A)** SPEI/MODIS-EVI and **B)** SPEI/MODIS-NDVI maximum Pearson correlation coefficients and the annual water balance across eco-regions. The biomes are grouped in six eco-regions: Subpolar, Boreal, Cool temperate, Warm temperate, Subtropical and Tropical. All the biomes are represented by the same symbol (circle).

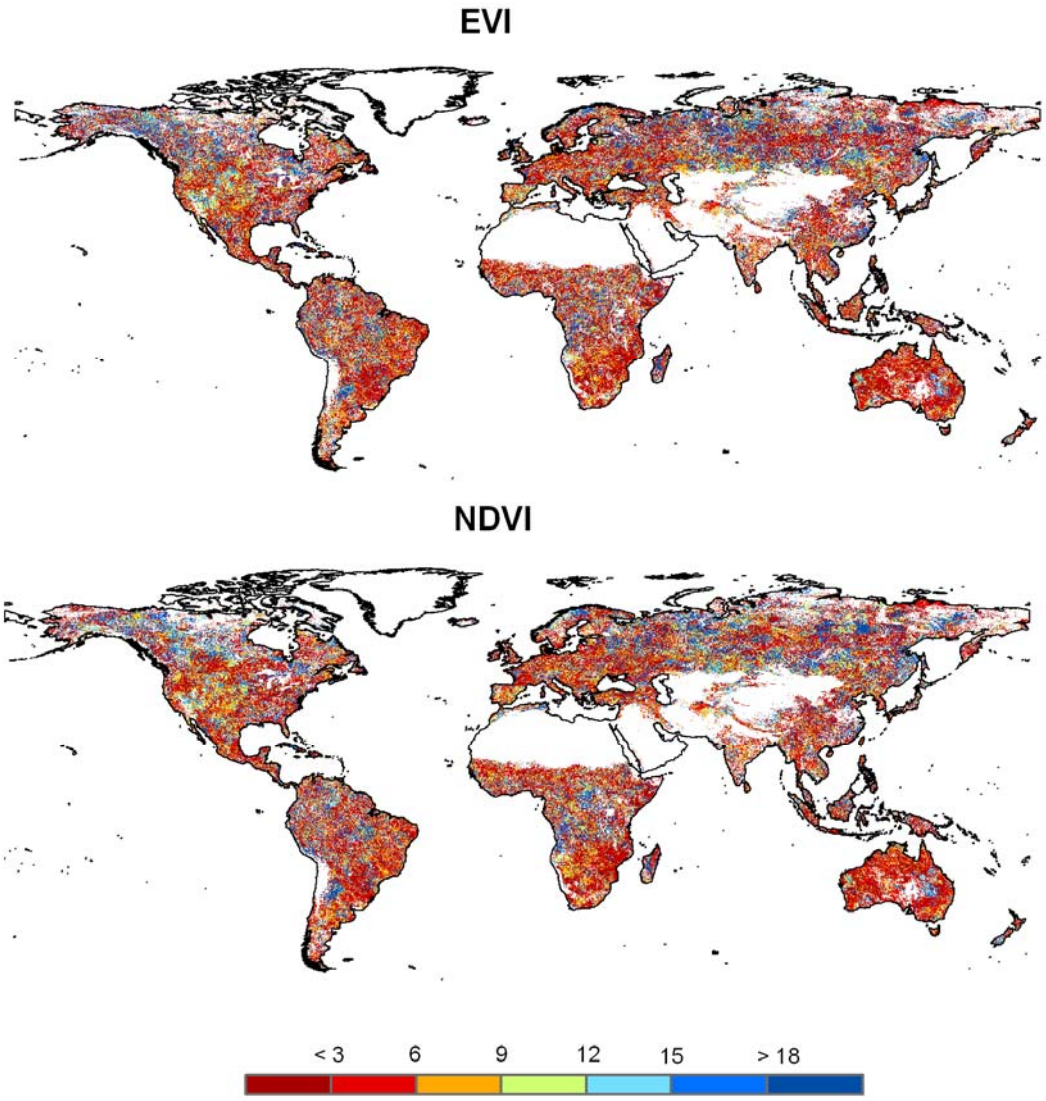

Figure S23. SPEI time scale (in months) at which the maximum correlation between SPEI and MODIS-EVI and MODIS-NDVI is found. Areas with no significant correlations are depicted in white. Desert and ice areas are masked and not included in the analyses.

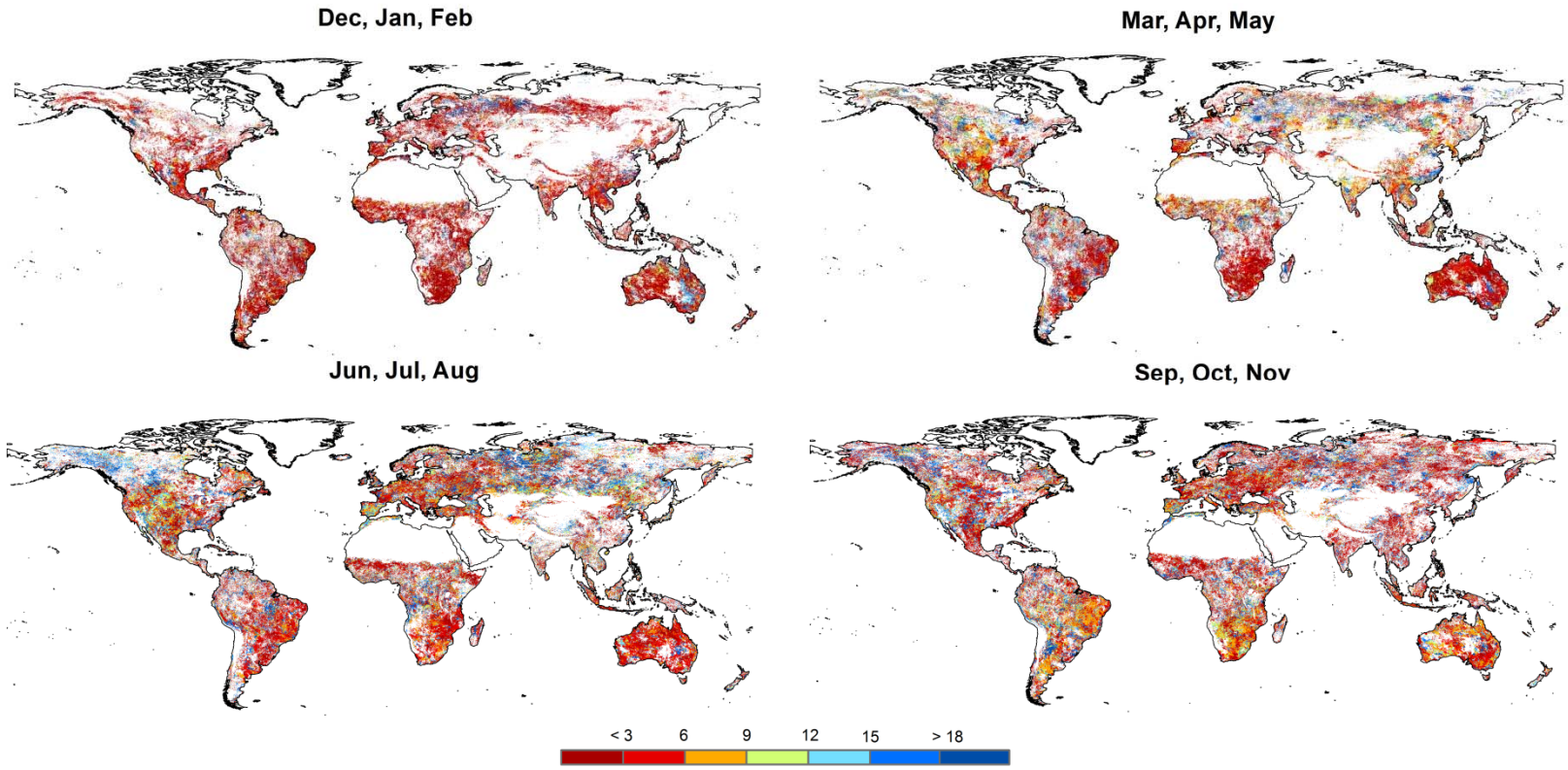

Figure S24. SPEI time scale (in months) at which the maximum seasonal correlation between SPEI and MODIS-EVI is found. Areas with no significant correlations are depicted in white. Desert and ice areas are masked and not included in the analyses.

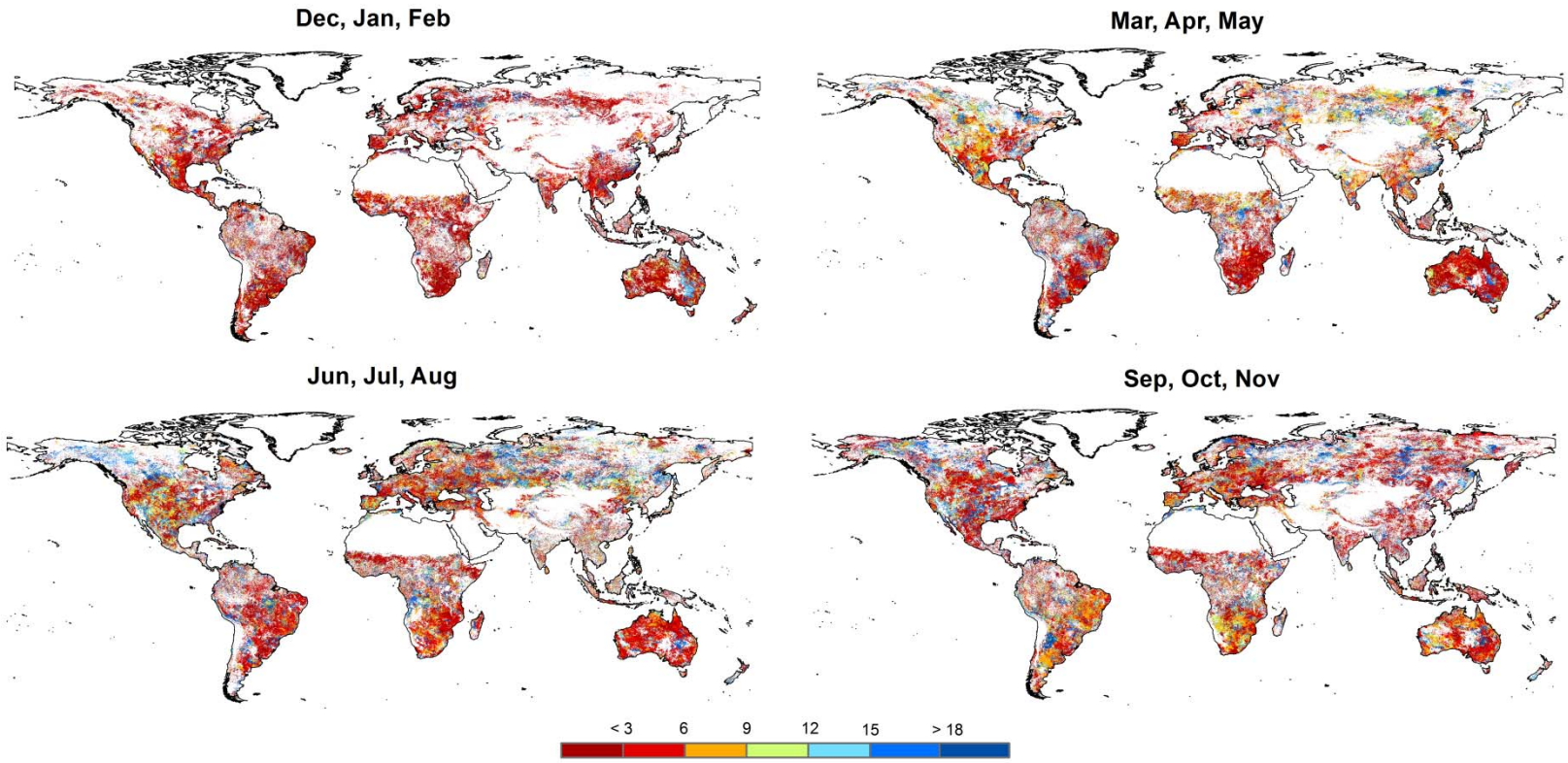

Figure S25. SPEI time scale (in moths) at which the maximum seasonal correlation between SPEI and MODIS-NDVI is found. Areas with no significant correlations are depicted in white. Desert and ice areas are masked and not included in the analysis.

5. Supplemental references

[S1]Heim RR (2002) A review of twentieth-century drought indices used in the United States. *Bulletin of the American Meteorological Society* 83: 1149-1165.

[S2]Keyantash J, Dracup J (2002) The quantification of drought: an evaluation of drought indices. *Bulletin of the American Meteorological Society* 83: 1167-1180.

[S3]Mishra AK, Singh VP (2010) A review of drought concepts. *Journal of Hydrology* 391: 202–216.

[S4]Sivakumar MVK, Motha RP, Wilhite DA, Wood DA (2010) Agricultural Drought Indices: Proceedings of an Expert Meeting, 2–4 June 2010, Murcia, Spain, 219 pp., World Meteorol. Org., Geneva, Switzerland.

[S5]Palmer WC (1965) *Meteorological droughts.* U.S. Department of Commerce Weather Bureau Research Paper 45, 58 pp.

[S6]McKee TBN, Doesken J, Kleist J (1993) The relationship of drought frecuency and duration to time scales. *Eight Conf. On Applied Climatology.* Anaheim, CA, Amer. Meteor. Soc. 179-184.

[S7]Guttman NB (1998) Comparing the Palmer drought index and the Standardized Precipitation Index. *Journal of the American Water Resources Association* 34: 113-121.

[S8]Hayes M, Wilhite DA, Svoboda M, Vanyarkho O (1999) Monitoring the 1996 drought using the Standardized Precipitation Index. *Bulletin of the American Meteorological Society* 80: 429-438.

[S9]Hayes M, Svoboda M, Wall N, Widhalm M (2011) The Lincoln Declaration on Drought Indices: Universal Meteorological Drought Index recommended, *Bulletin of the American Meteorological Society* 92: 485–488.

[S10]Szalai S, Szinell CS, Zoboki J (2000) Drought monitoring in Hungary. In *Early warning systems for drought preparedness and drought management.* World Meteorological Organization. Lisboa: 182-199.

[S11]Vicente-Serrano SM, López-Moreno JI (2005) Hydrological response to different time scales of climatological drought: an evaluation of the standardized precipitation index in a mountainous Mediterranean basin. *Hydrology and Earth System Sciences* 9: 523-533.

[S12]Khan S, Gabriel HF, Rana T (2008) Standard precipitation index to track drought and assess impact of rainfall on watertables in irrigation areas. *Irrigation and Drainage Systems* 22: 159-177.

[S13]Fiorillo F, Guadagno FM (2010) Karst spring discharges analysis in relation to drought periods, using the SPI. *Water Resources Management* 24: 1867-1884.

[S14]Vicente-Serrano SM, Cuadrat JM, Romo A (2006) Early prediction of crop productions using drought indices at different time scales and remote sensing data: application in the Ebro valley (North-east Spain). *International Journal of Remote Sensing* 27: 511-518.

[S15]Quiring SM, Ganesh S (2010) Evaluating the utility of the Vegetation Condition Index (VCI) for monitoring meteorological drought in Texas. *Agricultural and Forest Meteorology* 150: 330-339.

[S16]Abramopoulos F, Rosenzweig C, Choudhury B (1998) Improved ground hydrology calculations for global climate models (GCMs): Soil water movement and evapotranspiration. *Journal of Climate* 1: 921–941.

[S17]Williams AP, Xu Ch, McDowell NG (2011) Who is the new sheriff in town regulating boreal forest growth?. *Environmental Research letters* 6: doi: 10.1088/1748-9326/6/4/041004.

[S18]Martínez-Villalta J, López BC, Adell N, Badiella L, Ninyerola M (2008) Twentieth century increase of Scots pine radial growth in NE Spain shows strong climate interactions. *Global Change Biology* 14: 2868–2881.

[S19]Vicente-Serrano SM, Lasanta T, Gracia C (2010) Aridification determines changes in leaf activity in Pinus halepensis forests under semiarid Mediterranean climate conditions. *Agricultural and Forest Meteorology* 150: 614-628.

[S20]McGuire AD, et al. (2010) Vulnerability of white spruvce tree growth in interior Alaska in response to climate variability: ddendrochronological, demographic, and experimental perspectives. *Canadian Journal of Forest Research,* 40: 1197-1209.

[S21]Linares JC, Camarero JJ (2011) From pattern to process: linking intrinsic water-use efficiency to drought-induced forest decline. *Global Change Biology* 18: 1000-1015.

[S22]Rebetez M, et al. (2006) Heat and drought 2003 in Europe: A climate synthesis. *Annals of Forest Science* 63: 569-577.

[S23]Barriopedro D, Fischer EM, Luterbacher J, Trigo RM, García-Herrera R (2011) The hot summer of 2010: Redrawing the temperature record map of Europe. *Science* 332: 220-224.

[S24]Lobell DB, Schlenker W, Costa-Roberts J (2011) Climate trends and global crop production since 1980. *Science* 29: 616-620.

[S25]Vicente-Serrano SM, Beguería S, López-Moreno JI, Angulo M, El Kenawy A (2010) A new global 0.5° gridded dataset (1901-2006) of a multiscalar drought index: comparison with current drought index datasets based on the Palmer Drought Severity Index. *Journal of Hydrometeorology* 11: 1033–1043.

[S26]Köppen W (1936) Das Geographische System der Klimate. In Köppen, C.W. & Geiger, R., eds., Handbuch der Klimatologie ,vol. 3. Berlin:Gebrüder Bornträger.

[S27]Thornthwaite CW (1948) An approach toward a rational classification of climate. *Geographical Review* 38: 55-94.

[S28]Budyko MI (1974) *Climate and life*, Academic, New York.

[S29]UNEP (1992) World Atlas of Desertification. Edward Arnold. London.

[S30]Knipling EB (1970) Physical and physiological basis for the reflectance of visible and near-infrared radiation from vegetation. *Remote Sensing of Environment* 1: 155-159.

[S31]McVicar TR, Jupp DLB (1998) The current and potential operational uses of remote sensing to aid decisions on drought exceptional circumstances in Australia: a review. *Agricultural Systems* 57: 399-468.

[S32]Tucker CJ (1979) Red and photographic infrared linear combinations for monitoring vegetation. *Remote Sensing of Environment* 8: 127-150.

[S33]Bannari A, Morin D, Bonn F, Huete AR (1995) A review of vegetation indices. *Remote Sensing Reviews* 13: 95–120.

[S34]Baret F, Guyot G (1991) Potential and limits of vegetation indices for LAI and APAR assessment. *Remote Sensing of Environment* 35: 161–173.

[S35]Rouse JW, et al. (1974) *Monitoring the vernal advancement and retrogradation (greenwave effect) of natural vegetation.* NASA/GSFC type III Final Report, Greenbelt, MD.

[S36]Curran PJ (1980) Multispectral remote sensing of vegetation amount. *Progress in Physical Geography* 4: 315-341.

[S37]Holben BN, Tucker CJ, Fan C-J (1980) Spectral assessment of soybean leaf area and lear biomass.

Photogrammetric Engineering & Remote Sensing 46: 651-656.

[S38]Tucker CJ, Vanpraet CL, Sharman MJ, Van Ittersum G (1985) satellite remote sensing of total herbaceous biomass production in the Senegalese Sahel: 1980-1984. *Remote Senisng of Environment* 17: 233-249.

[S39]Myneni RB, et al (1995) Optical remote sensing of vegetation: modelling, caveats and algortihms. *Remote Sensing of Environment* 51: 169-188.

[S40]Hatfield JL, Asrar G, Kanemasu ET (1984) Intercepted photosynthetically active radiation estimated by spectral reflectance. *Remote Sensing of Environment* 14: 65-75.

[S41]Gallo KP, Daughtry CST, Bauer ME (1985) Spectral estimation of absorbed photosinthetically active radiation in corn canopies. *Remote Sensing of Environment* 17: 221-232.

[S42]Carlson TN, Perry EM, Schumugge TJ (1990) Remote estimation of soil moisture availability and fractional vegetation cover for agricultural fields. *Agricultural and Forest Meteorology* 52: 45-69.

[S43]Spanner MA, Pierce LL, Running SW, Peterson DL (1990) The seasonality of AVHRR data of temperate coniferous forests: relationship with leaf area index. *Remote Sensing of Environment* 33: 97-112.

[S44]Carlson TN, Ripley DA (1997) On the relation between NDVI, fractional vegetation cover, and leaf area index. *Remote Sensing of Environment* 62: 241-252.

[S45]Tucker CJ, Holben BN, Elgin JH, McMurtrey JE (1981) Remote Sensing of total dry matter accumulation in winter wheat. *Remote Sensing of Environment* 11: 171-189.

[S46]Tucker CJ, Vanpraet C, Boerwinkel E, Gaton A. (1981) Satellite remote sensing of total dry matter accummulation in winter wheat. *Remote Sensing of Environment* 11: 171-189.

[S47]Cihlar J, StLaurent L, Dyer JA (1991) The relation between normalized difference vegetation index and ecological variables. *Remote Sensing of Environment* 35: 279-298.

[S48]Gutman GG (1991) Vegetation indices from AVHRR. An update and future prospects. *Remote Sensing of Environment* 35: 121-136.

[S49]Asner GP, Alencar A (2010) Drought impacts on the Amazon forest: the remote sensing perspective. *New Phytologist* 187: 569-578.

[S50]Gutman GG (1990) Towards monitoring droughts from space. *Journal of Climate* 3: 282-295.

[S51]Che N, Price JC (1992) Survey of radiometric calibration results and method for visible and near infrared channels of NOAA –7, -9 and –11 AVHRRs. *Remote Sensing of Environment* 41: 19-27.

[S52]Schultz PA, Halpert MS (1995) Global analysis of the relationships among a vegetation index. Precipitation and land surface temperature. *International Journal of Remote Sensing* 16: 2755-2777.

[S53]Beck H, et al. (2011) Global evaluation of four AVHRR-NDVI data sets: Intercomparison and assessment against Landsat imagery. *Remote Sensing of Environment* 115: 2547-2563.

[S54]Justice DH, et al. (1998) The Moderate Resolution Imaging Spectroradiometer (MODIS): land remote sensing for global change research. *IEEE Transactions on Geoscience and Remote Sensing* 36: 1228–1249.

[S55] Huete A, et al. (2002) Overview of the radiometric and biophysical performance of the MODIS vegetation indices. *Remote Sensing of Environment* 83: 195-213.

[S56]Gao X, Huete AR, Ni W, Miura T (2000) Optical-biophysical relationships of vegetation spectra without background contamination. *Remote Sensing of Environment* 74: 609-620.

[S57] Didan K, Huete AH (2006) MODIS Vegetation Index Product Series Collection 5 Change Summary TBRS Lab., The University of Arizona June 29th, 2006. http://landqa2.nascom.nasa.gov/QA_WWW/forPage/MOD13_VI_C5_Changes_Document_06_28_06.pdf.

[S58]Grissino-Mayer HD, Fritts HC (1997) The International Tree-Ring Data Bank: an enhanced global database serving the global scientific community. *The Holocene* 7: 235-238.

[S59]Stokes MA, Smiley TL (1968) *An introduction to tree ring dating*. The University of Chicago Press, Chicago.

[S60]Holmes RL (1983) Computer-assisted quality control in tree-ring dating and measurement. *Tree-Ring Bulletin* 43: 69-78.

[S61]Brewer PW, Murphy D, Jansma E (2011) Tricycle: A Universal Conversion Tool For Digital Tree-Ring Data. *Tree-Ring Research* 67: 135-144.

[S62]Williams AP, et al. (2010) Forest responses to increasing aridity and warmth in the southwestern United States. *Proceedings of the National Academy of Sciences of the United States of America,* doi: 10.1073/pnas.0914211107.

[S63]Cook ER, Krusic PJ (2005) Program Arstan, a tree-ring standardization program based on detrending and autoregressive time series modeling, with interactive graphics. Tree-ring Laboratory Lamont Doherty Earth Observatory of Columbia University, Palisades, NY.

[S64]Murphy AH (1970) Predicted forage yields based on fall precipitation in California annual grasslands. *Journal of Range Management* 23: 363-365.

[S65]Passey HB, Hugie VK, Williams EW, Ball DE (1982) *Relationships between soil, plant community, and climate on rangelands of the Intermountain West.* U.S. Department of Agriculture, Technical Bulletin No. 1669.

[S66]Frichnecht NC, Harris LE (1968) *Grazing intensities and systems on crested wheatgrass in central Utah. Response of vegetation and cattle.* US Department of Agriculture, Bulletin 1388, Washington DC.

[S67]Blaisdell J (1958) *Seasonal development and yield of native plants on the upper Snake River Plain and their relation to certain climatic factors.* United States Department of Agriculture Technical Bulletin 1190.

[S68]Smoliak S (1986) Influence of climatic conditions on production of *Stipa Bouteloua* prairie over a 50-year period. *Journal of Range Management* 39: 100-103.

[S69]Cable DR (1975) Influence of Precipitation on Perennial Grass Production in the Semidesert Southwest. *Ecology* 56: 981-986.

[S70]Khumalo G, Holechek J (2005) Relationships between Chihuahuan desert perennial grass production and precipitation. *Rangeland Ecology & Management* 58: 239-246.

[S71]Andales AA, Derner JD, Ahuja JR, Hart RH (2006) Strategic and Tactical Prediction of Forage Production in Northern Mixed-Grass Prairie. *Rangeland Ecological Management* 59: 576–584.

[S72]Lauenroth WK, Sala OE (1992) Long-Term Forage Production of North American Shortgrass Steppe. *Ecological Applications* 2: 397-403.

[S73]Wight JP, Black AL (1979) range fertilization: plant response and water use. *Journal of Range Management* 32: 345-349.

[S74]Rogler GA, Haas HJ (1947) range production as related to soil moisture and precipitation on the northern Great plains. *Journal of the American Society of Agronomy* 38: 378-389.

[S75]Patton BD, Dong X, Nyren PE, Nyren A (2007) Effects of Grazing Intensity, Precipitation, and Temperature on Forage Production. *Rangeland Ecol Manage* 60: 656–665

[S76]Hulett GK, Tomanek GW (1968) Forage production on a clay upland range site in Western Kansas. *Journal of Range Management* 22: 270-276.

[S77]ORNL DAAC (2012) Net Primary Productivity (NPP) Data Sets. http://daac.ornl.gov/cgi-bin/dataset_lister.pl?p=13. Last access 10/04/2012.

[S78]Towne G, Owensby C (1984) Long term effects of annual burning at different dates in ungrazed kansas tallgrass prairie. *Journal of Range Management* 37*:* 392-397*.*

[S79]Bhattacharjee J, Haukos DA, Neaville J (2009) Influence of biotic and abiotic factors on annual aboveground biomass of an intermediate coastal marsh. *Wetlands* 29: 690-696.

[S80]Conner WH, Song B, Williams TM, Vernon JT (2011) Long-term tree productivity of a South Carolina coastal plain forest across a hydrology gradient. *Journal of Plant Ecology* 4: 67-76.

[S81]Jobbagy EG, Sala OE (2000) Controls of grass and shrub aboveground production in the Patagonian steppe. *Ecological Applications* 10: 541-549.

[S82]O'Connor TG, Haines LM, Snyman HA (2001) Influence of precipitation and species composition on phytomass of a semi-arid African grassland. *Journal of Ecology* 89: 850-860.

[S83]Tadmor NH, Eyal E, Benjamin RW (1974) Plant and sheep production on semiarid annual grassland in Israel. *Journal of Range Management* 27: 427-432.

[S84]Henkin Z, Seligman NG, Noy-Meir I (2010) Long-term productivity of Mediterranean herbaceous vegetation after a single phosphorus application. *Journal of Vegetation Science* 21: 979–991.

[S85]Bai Y, Han X, Wu J, Chen Z (2004) Ecosystem stability and compensatory effects in the Inner Mongolia grassland. *Nature* 431: 181-184.

[S86]Bentley JR, Talbot MW (1951) *Efficient use of annual plants on cattle ranges in the California foothills.* United States Department of Agriculture. Circular nº 870. Washington, D.C.

[S87]Fabrichon V (1997) Réaction de peuplements forestiers tropicaux a des interventions sylvicoles. *Bois et forêts del Tropiques* 254: 5-24.

[S88]Manokaran N, Kochummen KM (1987) Recruitment, Growth and Mortality of Tree Species in a Lowland Dipterocarp Forest in Peninsular. *Journal of Tropical Ecology* 3: 315-330.

[S89]Clark DA, Brown S, Kicklighter DW, Chambers JQ (2001) Measuring net primary production in forests: concept and field methods. *Ecological Applications* 11: 356–370.

[S90]Zweifel R, et al. (2010) Link between continuous stem radius changes and net ecosystem productivity of a subalpine Norway spruce forest in the Swiss Alps. *New Phytologist* 187: 819–830.

[S91]Etzold S, Ruehr NK, Zweifel R, Dobbertin M, Zingg A (2011) The carbon balance of two contrasting mountain forest ecosystems in Switzerland: similar annual trends, but seasonal differences. *Ecosystems* 14: 1289–1309.